CHARACTERIZATION OF THE EFFECTS OF REDUCED MUTANT HUNTINGTIN IN THE R6/1 MODEL OF HUNTINGTON'S DISEASE

By

EDGARDO RODRIGUEZ

A DISSERTATION PRESENTED TO THE GRADUATE SCHOOL
OF THE UNIVERSITY OF FLORIDA IN PARTIAL FULFILLMENT
OF THE REQUIREMENTS FOR THE DEGREE OF
DOCTOR OF PHILOSOPHY

UNIVERSITY OF FLORIDA

2005

I dedicate this work to my loving and ever-supportive wife Erica and my daughter Arianna; and to my parents, the inspiration of my life.

ACKNOWLEDGMENTS

I would like to acknowledge the support and enduring patience that my mentor, Dr. Ronald J. Mandel, had towards me from the beginning of this project. I also would like to make special mention of Dr. Alfred S. Lewin, whose wisdom and guidance made me the confident scientist that I am today. I would like to thank all of my committee members, Dr. Lucia Notterperk, Dr. Dennis Steindler and Dr. Nick Muzyczka for their insightfulness. I gratefully acknowledge the help and support from Dr. Eileen Denovan-Wright and her laboratory; she was that second pair of hands we all wish we had.

I thank everyone at the Mandel laboratory, especially Izzie Williams, for her technical and moral support. Special thanks go to my beloved friend Carmen Peden. I gratefully acknowledge all of the members of the Lewin laboratory, past and present, for their unconditional friendship and support. I also would like to thank Dr. Corinna Burger and Dr. Kevin Nash for lending me their time and for their ideas.

No words convey the gratitude that I have towards my parents. It is with much love that I acknowledge and deeply appreciate the sacrifices and difficulties that my loving wife, Erica, patiently endured. Lastly, but most importantly, I thank God for keeping us safe and healthy through it all.

TABLE OF CONTENTS

LIST OF FIGURES

Abstract of Dissertation Presented to the Graduate School
of the University of Florida in Partial Fulfillment of the
Requirements for the Degree of Doctor of Philosophy

CHARACTERIZATION OF THE EFFECTS OF REDUCED MUTANT HUNTINGTIN IN THE R6/1 MODEL OF HUNTINGTON'S DISEASE

By

Edgardo Rodriguez

August, 2005

Chair: Ronald J. Mandel
Major Department: Neuroscience

Huntington's disease (HD) is a fatal, inherited, autosomal dominant neurological disorder that currently affects over 30,000 individuals in the United States alone. HD is characterized by motor impairment and psychological manifestations. Expression of an abnormally expanded poly-glutamine domain in the N-terminus of the protein called huntingtin is responsible for the genesis and progression of the disease. The aim of this thesis was to develop molecular tools that could mediate the reduction in the levels of mutant huntingtin in the striatum of the R6/1 mouse model of HD. We hypothesized that reduced levels of striatal mutant huntingtin would ameliorate the progressive HD-like phenotype that is observed in the R6/1 mouse.

Our initial studies focused on the development of RNA enzymes, called ribozymes, and their ability to specifically target and efficiently knockdown the levels of mutant huntingtin *in vivo*. We found that, although anti-mutant huntingtin ribozymes were highly efficient *in vitro*, expression in the R6/1 striatum led to neuronal dysfunction in both

wild-type and R6/1 mice. Attempts at re-designing new ribozymes were hindered by limitations in target site accessibility and availability. Thus, we focused our efforts towards developing a new gene knockdown strategy based on the RNA interference pathway.

In vivo expression of anti-mutant huntingtin short-hairpin RNA molecules resulted in a significant reduction in the levels of striatal mutant huntingtin protein in the R6/1 mouse brain. This reduction was associated with a partial clearance of neuronal intranuclear inclusions. In addition, reduced levels of mutant huntingtin led to an increase in the levels of two neuronal-specific transcripts known to be downregulated in HD. Last, there was a delay in the onset of the rear paw clasping progressive phenotype observed in the R6/1 mouse.

These results demonstrate that reduced levels of striatal mutant huntingtin are beneficial in a genetic model of HD. Furthermore, the studies presented here address the therapeutic potential of RNA interference in the treatment of dominant disease. Finally, our ribozyme studies suggest the existence of an unidentified gene, or genes, whose expression is critical for the proper function of striatal neurons in the mouse brain.

CHAPTER 1
INTRODUCTION

Huntington's Disease

In 1872 a young American physician named George Huntington Jr. accurately described the symptoms of chorea and dementia as well as the adult-onset and genetic inheritance associated with the disease that would ultimately come to bear his name (40, 62). HUNTINGTON'S DISEASE (HD) is an inherited, autosomal dominant neurological disorder characterized by choreiform abnormal movements, cognitive deficits and pshychiatric manifestations associated with progressive striatal atrophy (3, 11). Formerly known as Huntington's chorea, HD affects approximately 1 in every 10,000 individuals of Caucasian origin with close to 30,000 HD patients currently diagnosed in the United States alone. There are at least 150,000 individuals who currently live with a 50 percent chance of developing HD, as well as thousands of family members and friends that must take on the challenge of caring for those with such a chronic devastating disease. Although HD was first described over a century ago, there is currently no effective therapy and, in the case of adult onset HD, the disease always leads to death within 10 to 15 years after the onset of symptoms (11, 97).

Huntington's disease affects different brain regions to various degrees; however, the neuropathological hallmark of HD is the enlargement of the lateral ventricles (3). Expression of the *HD* mutant gene leads to the selective degeneration of the gamma-amino-butyric-acid (GABA) medium sized spiny neurons that reside in the caudate-

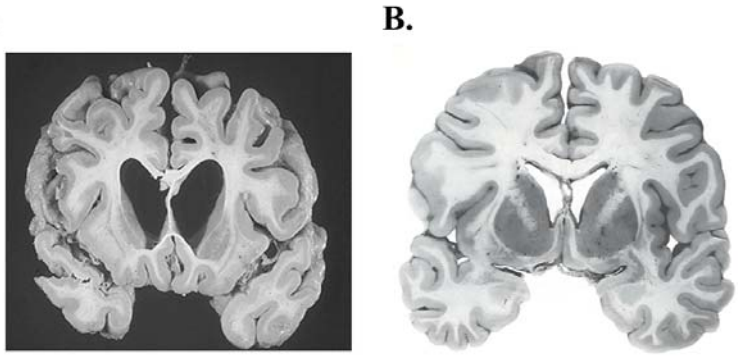

Figure 1-1. Neuropathology in HD. Panel (A) is a coronal section obtained from the brain of an HD affected individual. Notice the striatal degeneration that results in enlarged ventricles. Panel (B) is shown to demonstrate the size of the striatum in a normal brain.

putamen nucleus (striatum) (Fig. 1-1). This marked striatal susceptibility is not fully understood and although it results in gross neuroanatomical damage, it is only evident during the later stages of HD and it is not solely responsible for the etiology of the disease (45, 78). In fact, symptoms associated with HD are evident prior to any detectable striatal atrophy (45, 60). These symptoms, which include involuntary twitching, lack of coordination, depression, mood swings and forgetfulness, typically arise during mid-life (35-40 years of age) although close to 10 percent of affected individuals develop a more severe and aggressive form of the disease termed Juvenile HD, in which symptoms are evident before the age of 20 (94). The onset of symptoms prior to any significant cell loss, a phenomenon observed also in several animal models of the disease (7, 74, 84), suggests that neuronal dysfunction, and not cell death, is responsible for the initial stages of HD.

Genetics of HD

The advancements in modern molecular techniques during the 1980s and the unprecedented collaborative effort between groups of scientists from different institutions led to the discovery of the HD gene in 1993 (81). The study found that HD is caused by the inheritance of an unstable and excessively repeated cytosine-adenine-guanine (CAG) codon within the coding sequence in exon 1 of the *IT-15* gene (*HD* gene). Unaffected individuals were found to have repeats with lengths of 34 CAGs or less, while HD affected individuals had anywhere between 40 to 121 repeats. In HD, the severity of symptoms seems to be correlated with the number of repeats while the age of onset appears to be inversely proportional to the repeat amount (69), however, recent data obtained from the largest known HD kindred (50,000 individuals in Lake Maracaibo, Venezuela) suggest that genetic modifiers influence both severity and age of onset (90).

HD is developed when the CAG expansion is translated into a poly-glutamine (pQ) repeat domain in the N-terminus of the protein encoded by the *HD* gene named *huntingtin* (Htt) (81). Expression of expanded mutant Htt (m-Htt) results in the initiation of a cascade of events that progressively disrupt neuronal homeostasis. Importantly, expression of the expanded *HD* gene leads to activation of caspases, which in turn cleave m-Htt into small N-terminal pQ-containing fragments (46, 61). These fragments can readily cross through the nuclear pore and become aggregated inside the nucleus. Abnormal nuclear translocation of expanded m-Htt N-terminal fragments is required for the pQ-induced cell death observed in cellular models of HD (73).

Huntingtin

Huntingtin is a large, 348 kDa, cytoplasmic protein of unknown function. It is localized to many subcellular compartments and expressed in all tissues of the body with

Figure 1-2. Structure domains of huntingtin. Shown above is a depiction of the structure domains present in huntingtin. The poly-glutamine domain (pQ) lies just upstream of a poly-proline rich domain (pp). A stretch of 36 HEAT-like domains is thought to serve as docking sites for cellular proteins.

higher concentrations found in the brain and testis (24, 50). Htt has three major domains: a polymorphic poly-glutamine domain, a proline-rich domain and 36 HEAT-like repeat structures (Fig, 1-2); however, its amino-acid sequence has no major homology to any known protein (75). Even though Htt's function has been difficult to elucidate, new insights have emerged from studies in culture and animal models of HD.

Initially, approaches to the study of Htt's function focused on the disruption of the murine HD homolog gene (*Hdh*). Ablation of the *Hdh* gene in the mouse results in embryonic lethality associated with aberrant brain development and increased apoptotic cell death , while post-natal conditional deletion in the mouse forebrain leads to abnormal brain development and neurodegeneration reminiscent of HD (19, 95). These observations suggest a critical role for Htt during neurogenesis and development. Recent evidence suggests that Htt may function as a scaffolding protein (50, 66) and that it is involved in many cellular processes such as neuronal vesicle transport in both the endocytic and secretory pathways, protein trafficking and transcriptional regulation (13). Studies have demonstrated that Htt colocalizes with vesicles and that expression of m-Htt can interfere with normal neuronal vesicular transport (24). Additionally, Htt was found to be a crucial member of the dynactin complex and this interaction was required for the proper cortico-striatal anterograde transport of brain-derived neurotrophic factor (BDNF) (24, 38). Also, wild-type Htt is proposed to have anti-apoptotic properties and may play a

role in neuronal survival (87). The abnormal level of apoptotic cells found in the *Hdh* knockout mouse supports this hypothesis. Finally, it was recently showed that Htt interacts with the REST-NRSF complex and that this interaction promotes the expression of neuron specific genes such as BDNF (97). Taken together, these data suggest a complex cellular role for Htt; however, what that specific role is, remains inadequately explained.

CAG Triplet Repeat Disorders

The presence of a pQ domain in m-Htt makes HD a member of a family of at least nine neurological disorders known as the CAG triplet repeat or pQ repeat disorders which include Dentato-rubral pallido-luysian atrophy (DRPLA), Spinobulbar muscular atrophy (SBMA) and the Spino-cerebellar ataxias (SCA) 1, 2, 3, 6, 7 and 17 (20, 23). Although all of these disorders differ in the context of the protein containing the pQ domain, they share many similarities including threshold CAG expansion lengths, genetic inheritance, adult-onset and progressive neurodegeneration (23, 28, 65). Additionally, all of these disorders are well characterized by the aberrant nuclear translocation of the mutant protein as well as by the abnormal aggregation of cellular proteins that results in the formation of intracellular bodies both in and outside the nucleus known as inclusion bodies (30, 71, 89).

Neuronal Inclusion Bodies

Many of the known neurodegenerative disorders such as HD, Parkinson's disease, Alzheimer's disease and amyotrophic lateral sclerosis (ALS) are characterized by the presence of proteinaceous bodies readily visible under the light microscope. In the case of HD, insoluble protein aggregates are observed late in the progression of disease (7, 70, 85, 87). It has been suggested that this process is modulated by the activation of caspases

that mediate the cleavage of m-Htt into small, toxic and aggregate-prone N-terminal fragments (88). m-Htt sequesters into these inclusions, proteins that are critical for maintaining neuronal homeostasis, i.e., transcription factors such as Sp1, effectively interfering with their proper cellular localization and function (14). This sequestration is proposed to take place via a variety of different mechanisms such as the formation of polar-zipper structures, transglutamination and SH3-domain dependent binding, all resulting in aberrant protein-protein interactions that take place in and are modulated by the pQ domain region of m-Htt (7, 66). Also, it has been suggested that inclusion bodies can lead to neurite and neuropil dystrophy and can physically interfere with cellular processes critical for neuronal function such as protein transport and proteosomal processing (11, 32, 49, 50).

In contrast, other researchers have proposed that the formation of inclusion bodies in HD is a neuronal defense mechanism designed to neutralize the toxicity associated with the expanded pQ domain in m-Htt. In fact, a strong correlation between the formation of inclusion bodies and survival rate was recently observed in neurons engineered to express m-Htt in culture (2, 63). Whether the presence of inclusion bodies in HD forms an integral part of the disease process itself or is an attempt by neurons to cope with an otherwise toxic protein remains controversial. Nevertheless, many agree that inclusion bodies are a reliable marker of disease progression and suggest a common pathological mechanism amongst many neurological disorders (6, 63).

Transcriptional Dysregulation in HD

Transcriptional dysregulation has recently been suggested as an important pathogenic mechanimsm in HD (12, 14, 51, 79). Both HD models and patients display a progressive loss in steady-state mRNA levels of a subset of striatal neuronal transcripts

(14, 79). Recent observations implicate the formation of intranuclear inclusions and the sequestration of transcription factors into aggregates as possible explanations for the loss in gene transcription (14). There is mounting evidence suggesting that soluble forms of mutant huntingtin alter the expression of specific genes by interacting with their transcriptional activators (55). X-ray diffraction studies have shown that the poly-glutamine domain in m-Htt can mediate the aberrant interaction between m-Htt and poly-glutamine-containing transcription factors via the formation of polar-zipper structures in vitro (66). In addition, yeast-two hybrid screens have illustrated m-Htt's interaction with several transcription factors such as p53, SP1 and the CREB-binding protein (CBP) in vivo (74). This evidence suggests that the specific interaction of m-Htt with factors that control transcriptional activation results in the early and progressive loss of striatal-specific mRNAs in HD**.**

The cyclicAMP-responsive element (CRE) -mediated transcription pathway is impaired in HD (11, 24, 75). CRE-mediated transcription is activated by the interaction between phosphorylated CREB and CBP. This results in the recruitment of the transcriptional machinery and initiates transcription. In HD, the transcriptional co-activator CBP is recruited into m-Htt aggregates and leads to inhibition of CBP-mediated transcription as well as cellular toxicity (41, 55). Overexpression of CBP can alleviate the toxicity associated with the expression of m-Htt in a neuroblastoma cell line. In addition, m-Htt can also sequester $TAF_{II}130$, a critical regulator of CBP, CRE-mediated transcription, into aggregates (14). These observations suggest that m-Htt expression can block the proper targeting of the transcriptional machinery to CRE-dependent promoters in affected neurons, resulting in the loss of transcriptional activity.

The interaction between m-Htt and regulators of transcription may provide evidence of the "gain of toxic" function associated with the abnormally expanded pQ domain in Htt. However, although the interruption on neuronal transcription happens early in the evolution of the disease, the role that this plays in the molecular cascade initiated by expression of m-Htt remains unresolved.

Transgenic Models of HD

The characterization of the mutation responsible for the neurological phenotype observed in HD in 1993 led to the report of the first successful HD transgenic mouse line, the R6 line, three years later (54). Since then, several transgenic and knockin lines have been developed that accurately portray the progressive phenotype associated with HD (7, 72). All of these have in common the expression of an expanded CAG repeat although they differ in the genetic context in which the abnormal expansion is expressed. Importantly, the onset, rate of progression and severity of motor symptoms displayed by these models are dependent on the number of repeats and the levels of m-Htt protein expression. Of all the lines generated to date, the R6/1 and R6/2 transgenic lines remain the best characterized.

In both patients and transgenic HD mice, the age of onset, disease progression and severity of symptoms are correlated with the expression of m-Htt and the length of the trinucleotide CAG repeat. The R6 HD transgenic lines, R6/1 and R6/2, were created by inserting a transgene containing the 5'-untranslated region, exon1 with an expanded CAG repeat, and part of the first intron of the human *HD* gene. This transgene is under the control of the human HD promoter and generates a short N-terminal fragment with an expanded pQ domain. Differences between the R6/1 and the R6/2 transgenic lines include the length of the CAG repeat (R6/2 > R6/1) and the site of integration of the

transgene, thought to result in differences in the amount of protein produced (R6/2>R6/1) (54, 72). R6/1 mice have a slower disease progression and a later onset of motor abnormalities than the R6/2 mice. Previous work demonstrated that levels of m-Htt protein are lower in the R6/1 mice compared to R6/2 and that neuronal intranuclear inclusions (NIIs) form more slowly throughout the brain tissue in R6/1 compared to R6/2 mice (7, 54, 72). Therefore, the length of the polyglutamine tract encoded by the human *HD* transgene and the relative levels of expression of the transgene affect the rate of HD progression in these mice. The relatively slower rate of disease progression and longer lifespan of the R6/1 mice make them more amenable for the study of slow acting interventions. In this study, we focus on the use of R6/1 mice.

The R6/1 transgenic line is characterized by an early onset of pQ-associated changes in neuronal function and a slow progression of motor phenotype. These mice exhibit decreased striatal and total brain size; however reports of neuronal death have been contradictory (7, 38). R6/1 mice also display ubiquitinated nuclear and cytoplasmic neuronal inclusion bodies containing both mutant and wild-type Htt. Also, there is increasing evidence of transcriptional dysregulation, which is modulated by the CAG expansion and levels of transgene expression (36, 56). Finally, the expression of expanded m-Htt results in the development of a neurological phenotype in 15 week-old R6/1 mice, a much earlier time point than was initially reported. R6/1 mice exhibit several behavioral abnormalities including gait disturbances, progressive clasping of the hindlimbs and seizure activity, all associated with neuronal dysfunction (10, 58). Finally, a failure to maintain body weight, as well as muscle wasting, has been reported.

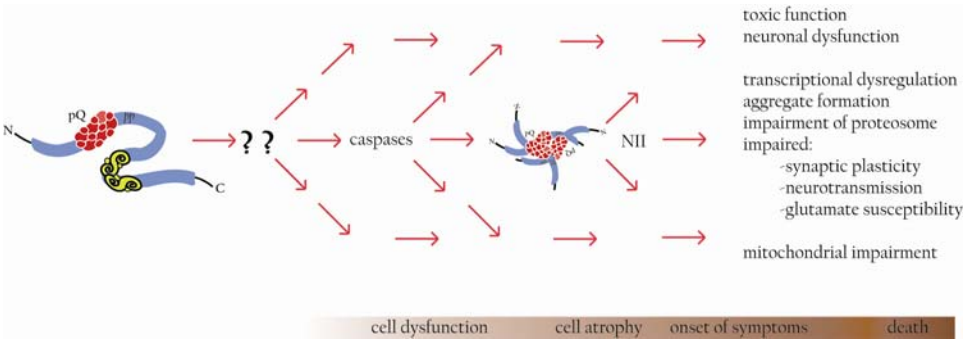

Figure 1-3. Molecular cascades in HD**.** The interaction of expanded m-Htt with unknown cellular proteins leads to divergent pathways that ultimately result in neuronal pathology. Activation of caspases appears to be an early step in the progression of disease. m-Htt fragments lead to the formation of neuronal intranuclear inclusions (NII) which normally appear just prior to the onset of symptoms. A diagram of disease progression is shown in bottom of the figure.

Gain of Function vs. Loss of Function

Although HD is a monogenic disorder, it has proven difficult to unravel the pathological mechanism that results in the development of disease. Many molecular pathways that lead to neuronal dysfunction and cell death have been proposed; however, the temporal relationship between these mechanisms and disease progression remains controversial (6, 14, 72). Figure 1-3 is a pictorial representation of the downstream neuronal consequences of m-Htt expression. Independently from downstream effects, the expression of an expanded pQ in m-Htt is directly responsible for the development of HD. However, Htt's normal function has remained elusive, greatly hindering the interpretation of data obtained from both cellular and animal models of disease. In order to identify the immediate downstream effectors of m-Htt action, we must gain a detailed understanding of the role that both wild-type and m-Htt play in neuronal function.

The recent data on Htt's wild type function and its role in neuronal development and survival support a model in which the loss of wild type function is responsible for the pathological molecular process that leads to HD. This model suggests that in homozygote

individuals the absence of a wild-type *HD* allele may progressively lead to neuronal dysfunction and eventual susceptibility to insults, while in heterozygote patients, mutant Htt may act in a dominant negative fashion against the wild type allele, effectively interfering with the normal cellular function of wild-type Htt. This idea is further supported by the observation that wild-type Htt is also sequestered away into inclusion bodies by mutant Htt and appears to be depleted in both humans as well as animal models of HD (95).

In contrast, others favor the idea that the mechanism underlying the pathogenesis of HD is the gain of a new toxic function associated with the pQ expansion in mutant Htt (53). In support of this theory is the fact that individuals with a deletion in one HD allele do not develop HD (Wolf-Hirschorn syndrome) (53) and the observation that there is no significant difference in the severity of symptoms between homozygote and heterozygote HD patients (3). In fact, there is a stronger correlation between the severity of symptoms and the number of CAGs in the HD gene (29, 53, 90). Furthermore, as described earlier, mutant Htt is involved in aberrant protein-protein interactions that result in a disruption of normal neuronal processes in a time dependent manner. The fact that Htt's normal function remains elusive is a giant hurdle in the quest for the understanding of the molecular underpinnings of HD. It is likely that both models described above act in concert and are both responsible for the damage observed in HD. However, it is of vital importance to fully dissect the contributions of each during the disease process as this would lead to the development of more effective therapies such as those aimed at reducing the levels of Htt expression in the brain.

Nucleic Acid-Based Gene Therapy

The genesis and progression of disease in dominant genetic disorders require the expression of the mutant protein. In the case of HD, this concept was first demonstrated using a mouse model that carried an expanded *HD* allele engineered to shut down its expression under specific pharmacological conditions (91). This conditional model showed that the expression of m-Htt was necessary to maintain the progression of disease and that interruption of mutant Htt expression, while maintaining wild type levels of normal Htt, led to a reversal of HD-like symptoms including a clearance of inclusions and behavioral improvements. This observation led to the hypothesis that suppressing mutant Htt activity would ameliorate the HD phenotype in affected individuals. Although several pharmacology-based mechanisms may be employed to achieve suppression of gene expression, nucleic acid-based methods (NABM) are the most potent, specific and cost-effective way of achieving post-transcriptional suppression of m-Htt gene expression (18, 81, 82). Recent advances in molecular design and intracellular delivery of nucleic acids further enhance the application of NABM for the treatment of dominant neurological disorders. There are three different NABM that result in post-transcriptional gene silencing: anti-sense oligodeoxyribonucleotides (AODN), ribozymes and small-interfering RNAs (siRNA). This study focused on the use of small self-cleaving ribozymes and siRNAs in order to suppress m-Htt gene expression *in vivo*.

Ribozymes

Ribozymes are catalytic RNA molecules that mediate the sequence-specific cleavage of other RNA molecules (34, 35, 48). Ribonucleotide enzymes (ribozymes) catalyze the hydrolysis and phosphoryl exchange at the phosphodiester linkages between RNA bases resulting in cleavage of the substrate. There are three main groups of

ribozymes which are classified as follows based on function and size: self-splicing introns, Rnase P and small self-cleaving ribozymes (96). This study focused on the use of small self-cleaving hammerhead ribozymes, naturally occurring enzymatic RNAs that can catalyze the cleavage of RNA molecules in reactions that are devoid of proteins. The most commonly studied small ribozymes include the hammerhead, the hairpin and the hepatitis delta virus ribozymes (22, 48, 96). Of these three the hammerhead ribozymes display great versatility as a tool for the study of gene function and disease.

Hammerhead ribozymes are approximately 34 base-pairs in length and can mediate the cleavage of an RNA target in trans. The hammerhead ribozymes bind substrate to form a structure that consists of a stem and three loops and a catalytic core with a conserved nine- nucleotide sequence (96) (Fig. 1-4). Point mutations within the conserved region prevent the cleavage of RNA. The hammerhead ribozyme cleaves the substrate by a trans-esterification reaction, which is dependent on the presence of magnesium and water. The enzymatic reaction results in the formation of two products with distinct 3' (2'-3' cyclic phosphate group) and 5'ends (5'-hydroxyl group). Following the cleavage of the RNA backbone, the reaction products diffuse away from the active site leaving the ribozyme free to complete another reaction cycle. The hammerhead ribozyme recognizes substrate sequences on either side of a NUX triplet cleavage site, where N is any nucleotide and X is any nucleotide except G. The ribozyme anneals to the mRNA substrate by means of two flanking arms, which hybridize to form helices III and I (Fig 1-4). Cleavage occurs at the 3' end of the NUX site. There are varying degrees of cleavage efficiency associated with the sequence of the NUX triplet. Cleavage occurs at the 3' end of the NUX site.

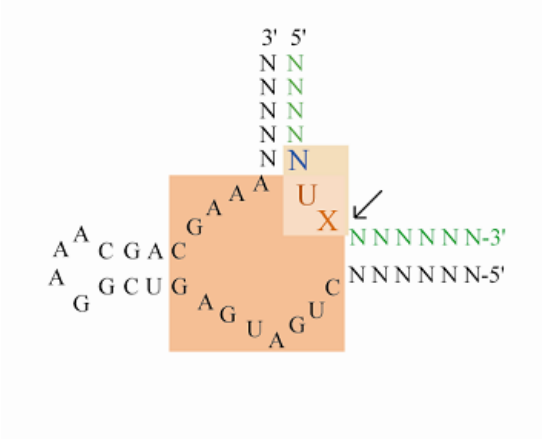

Figure 1-4. The hammerhead ribozyme. The hammerhead ribozyme binds substrate to form a structure, which consists of a stem and three loops and a catalytic core (shaded box) with a conserved nine-nucleotide sequence. The NUX cleavage site is indicated. The arrow denotes the site of bond cleavage.

There are varying degrees of cleavage efficiency associated with the sequence of the NUX triplet. In general, the triplet GUC is the most efficient cleavage site, followed by CUC, UUC and AUC (78). Other cleavage sites are cleaved at least 10 times less efficiently than the GUC site (77).

The turnover characteristic of ribozymes provides them with an advantage over standard antisense technology, which only inactivates the target RNA without degrading it. Due to their size, catalytic properties and lack of cellular toxicity, hammerhead ribozymes show great promise as tools in molecular medicine. In fact, the successful application of hammerhead and/or hairpin ribozymes in the treatment of dominant genetic disorders has been reported (48). Specifically, the use of hammerhead ribozymes against mutant rhodopsin was shown to effectively protect against photoreceptor degeneration in a mouse model of Retinitis Pigmentosa (47). Additionally, new gene regulation systems are being developed which incorporate the use of regulatory sequences called aptamers into existing hammerhead ribozymes (17, 68). This fusion of these technologies allows for the design of drug-responsive ribozymes, which only

catalyze the cleavage of target RNA in the absence of a regulatory drug while becoming inactive in the presence of the drug.

To date, ribozymes are being used in a variety of gene transfer strategies including the suppression of viral infection as well as in anti-oncogene strategies aimed at correcting cancer associated with genetic defect (22, 48, 96). The ease with which hammerhead ribozymes can be designed and regulated, coupled with the recent advances in viral gene delivery systems, give these small versatile molecules great potential as therapeutic agents.

RNA Interference

During recent years a new technology, called RNA interference (RNA*i*), has completely revolutionized the study of gene function and the design and application of nucleic acid-based therapies aimed at the silencing of disease-associated gene expression. RNA interference is an innate cellular process associated with immune surveillance as well as the regulation of gene expression during development in mammalian cells (82). This mechanism specifically responds to the presence of double-stranded RNA (dsRNA) molecules and directs the activity of post-transcriptional processes that lead to the sequence-specific inhibition of genes with complementary sequence to the dsRNA molecule (18). During RNAi, dsRNA molecules are rapidly processed by an enzyme called DICER into small duplex RNA molecules of 20 to 21-nucleotides in length called small-interfering RNAs (siRNA). Unidentified components of the RNA*i* machinery recognize and incorporate a single strand of the siRNA molecule into a ribonucleo-protein complex called the RNA-induced silencing comlex (RISC) (82, 83). RISC can then survey the mRNA population in order to mediate the sequence-specific cleavage of a target mRNA (Fig. 1-5).

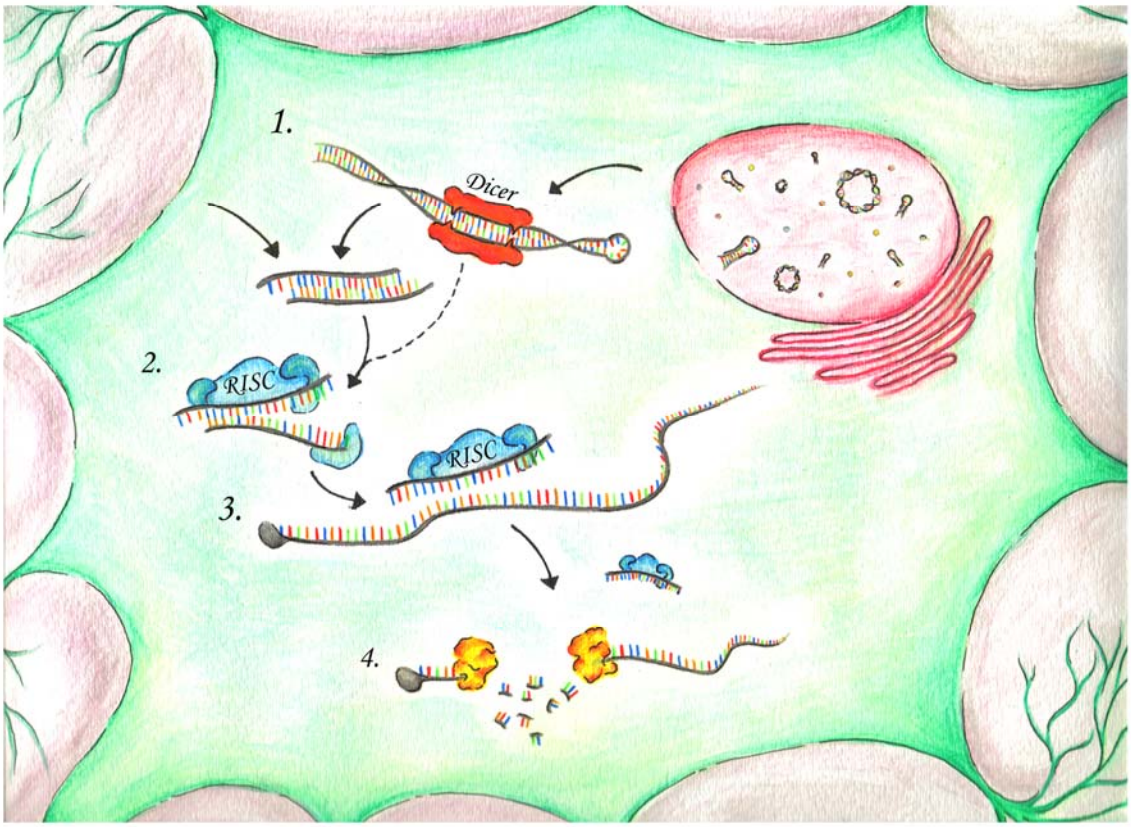

Figure 1-5. The RNAi pathway. Intracellular short-hairpin RNAs are processed by DICER (1) into small-interfering RNA molecules (siRNA). siRNAs are loaded into a ribonucleoprotein enzyme complex called RISC (2). The RISC/siRNA complex can mediate the sequence specific cleavage of an RNA molecule (3). This results in the degradation of the cleaved RNA by cellular nucleases. (Illustration by Erica L. Rodriguez)

This process can be experimentally manipulated by introducing synthetic siRNAs into the cell, which are then incorporated into RISC and mediate the silencing of the experimental gene of interest (18). Importantly, in mammalian cells the size of the siRNA molecule must not exceed 30-nucleotides in length, since siRNAs that exceed this threshold have been shown to activate the innate interferon response and lead to cell death (83). Additionally, methods for the intracellular expression of short-hairpin RNAs (shRNA) delivered as plasmid vectors have been recently developed (16, 18). shRNAs are expressed as fold-back stem-loop structures comprised of a sense and an antisense

strand and separated by a non-complimentary loop. The transcription of shRNAs is normally placed under the control of RNA polymerase III, which is capable of generating a transcript with a specified 3'-end terminal shown to be required for efficient silencing activity (18). Once transcribed by the nuclear machinery, shRNAs are exported into the cytoplasm, processed by DICER into functional siRNAs and incorporated into RISC.

Unlike anti-sense oligodeoxyribonucleotides (AODN) and ribozymes, siRNAs achieve the silencing of genes through an endogenous host-cell, anti-viral defense mechanism that has had the opportunity to evolve and become highly efficient over time. Additionally, siRNAs act in concert with the RISC protein complex, which results in increased stability and a more efficient capacity to turn over (18). Also, the stability of RNA duplexes allows for siRNAs to be readily delivered into cells and makes it possible to achieve biologically relevant concentrations inside the cell. Furthermore, low concentrations of highly active siRNAs have been shown to induce long-term gene silencing (82), making these molecules more pharmacologically attractive than either AODNs or ribozymes. However, although this is a potent molecular tool, RNA*i* is a relatively new and developing technology and unintended effects already known to be associated with it, such as changes in expression of non-targeted genes, must be carefully considered.

Gene Delivery in the CNS

Viral as well as non-viral vectors can be used to deliver therapeutic genes directly into the central nervous system (CNS) in a process termed *in vivo* gene transfer. Although non-viral vectors circumvent some of the potential toxic problems associated with viral vectors, it has been difficult to achieve and maintain high levels of transgene expression (43, 65). Viral vectors were designed based on the natural ability of viruses to infect,

transfer and express their genetic material in host cells. When compared to non-viral delivery methods, viral vectors are capable of mediating longer, more widespread and intense transgene expression in the CNS (16, 42, 64). The successful application of viral vectors in the CNS depends on the vector's capacity to mediate long-term transgene expression in non-dividing cells. In addition, the immunogenecity associated with the natural life cycle of the chosen vector most be assessed. Although different viral vectors have been successfully used in the CNS, our study focused on the use of recombinant Adeno-Associated viruses (rAAV).

The first rAAV vectors were described approximately 20 years ago (37). Since then, their use has revolutionized the study of genetic disease in the CNS by allowing the temporal and somatic regulation of gene expression (6, 8). AAV recombinant vectors are small, single-stranded DNA viruses capable of infecting both dividing and non-dividing cells (8, 37). Wild-type AAV is a non-pathological member of the *parvoviridae* family able to integrate its genome into the host's DNA. In contrast to its wild-type counterpart, rAAV integration events seem to occur less frequently and more randomly (1, 21, 43). rAAV vectors promote stable, long-term transgene expression in the CNS (4, 8). Moreover, CNS exposure to rAAV capsid proteins does not lead to cellular toxicity. However, the presence of circulating antibodies can block rAAV transduction and can mediate a cellular immune response upon re-administration of the vector (86). Recently, three different pseudo-typed rAAV vectors (rAAV-1, rAAV-2 and rAAV-5) where found to efficiently transduce various regions of the rat CNS (13). The use of different pseudo-typed rAAV vectors allows for the development of protocols that can circumvent the

immunological problems associated with circulating antibodies and vector re-administration.

The remarkable ability of rAAV vectors to efficiently transduce and sustain the long-term expression of genes in neuronal tissue, with negligible induction of the immune response, have led to the development of a variety of clinical protocols aimed at the treatment of CNS disorders. Some of these gene transfer strategies include gene replacement in Canavan's disease, Parkinson's disease and lysosomal storage disorders (15). Also, rAAV-based strategies for the delivery of neuroprotective factors in Alzheimer's, Huntington's and amyotrophic lateral sclerosis (ALS) have been reported (80). In conclusion, rAAV vectors can efficiently deliver genes into the CNS. rAAV holds the promise as the future vector of choice for the delivery of therapeutic genes in the clinic.

CHAPTER 2
RIBOZYME-MEDIATED REDUCTION OF STRIATAL MUTANT HUNTINGTIN IN VIVO

Introduction

The progressive striatal pathology observed in Huntington's disease patients is caused by the expression of an abnormally expanded poly-glutamine (pQ) domain in N-terminus of the ubiquitously expressed protein termed huntingtin (Htt) (29, 53). The uninterrupted expression of m-Htt is necessary for the genesis and evolution of HD as shown by a conditional transgenic mouse model expressing a CAG expanded HD transgene under the control of the tetracycline promoter (92). In this model, transcriptional suppression of m-Htt expression, in both cortical and striatal regions of the brain, led to a reversal of cellular and behavioral HD-like phenotype. However, the effect that reduced striatal levels of m-Htt would have on the phenotype of transgenic HD mice has not been assessed. We hypothesized that post-transcriptional knockdown of m-Htt should lead to an amelioration of the HD-like phenotype in the R6/1 transgenic mouse line. In vitro studies have demonstrated that anti-sense oligodeoxyribonucleotides directed against an expanded human HD allele can mediate the suppression of m-Htt protein expression in cultured cells (9, 33, 59). Similarly, DNA-enzymes, which are composed of a ribonucleotide catalytic frame placed in between deoxy-ribonucleotide hybridizing arms, were successfully used against m-Htt mRNA and resulted in specific suppression of m-Htt protein expression (93). These data suggest that, unlike other

proteins such as those involved in cell signaling, reduced intracellular levels of m-Htt do not induce HD promoter activity. More importantly, they demonstrate that the secondary structure of m-Htt mRNA contains biologically accessible regions for Watson-Crick base pairing. However, the application of these two technologies in in vivo models of HD is limited. First, high intracellular concentrations of anti-sense oligo-deoxy-ribonucleotides are required in order to achieve significant reduction of protein expression in vivo (9, 96). This leads to cellular toxicity and the induction of the immune response. Addionally, anti-sense molecules are fairly unstable and the mechanism by which they mediate gene silencing is currently unknown. Also, the efficient in vivo delivery and long-term expression of anti-sense molecules and DNAenzymes, which cannot be encoded for, represents a challenge that is not easily surmounted.

Hammerhead ribozymes are RNA enzymes that can be targeted to catalyze the cleavage of a specific RNA molecule (5, 48, 96). High intracellular concentrations of hammerhead ribozymes are not toxic and can be achieved with vector-based expression systems (34, 47, 48). Ribozymes against the untranslated 5'end region of the HIV-1 genome have been shown to inhibit virus replication (5). Moreover, rAAV-mediated delivery of a hammerhead ribozyme against mutant rhodopsin mRNA resulted in the rescue of photoreceptors in a mouse model of retinitis pigmentosa (47). These results suggest that hammerhead ribozymes can efficiently mediate the knockdown of target RNAs *in vivo*.

In this study, we examined the effects of ribozyme-mediated post-transcriptional suppression of striatal m-Htt in the R6/1 mouse. We specifically assessed whether rAAV-ribozyme expression could affect the transcriptional dysregulation phenotype that is

associated with the expression of m-Htt in the R6/1 mouse striatum. *In vitro* screening of ribozymes against the *HD* transgene expressed in the R6/1 mouse resulted in the identification of two highly active ribozymes. Surprisingly, rAAV-mediated expression of these two ribozymes in the striatum of either R6/1 or age-matched wild-type mice resulted in a marked decrease in the steady-state levels of pre-pro-enkephalin (ppEnk), dompamine- and cAMP-regulated phosphoprotein of 32 kDa (DARPP-32) and the dompamine receptor type-2 (D2R) mRNAs. We report that ribozymes targeting a region just upstream of the CAG repeat domain in the human Htt mRNA mediate the cleavage of an unidentified RNA molecule critical for neuronal function and survival.

Materials and Methods

Defining Target Sites

Target sites containing a GUC (HD6 and HD7), CUC (dsCAG1) or UUC (dsCAG2) cleavage site were chosen from the human exon 1 Htt mRNA sequence (Genbank accession number L27350). Target regions with six nucleotides on either side of the arms consisting of a 50% GC content were selected since an ideal length for the target region is between 6-7 nucleotides. The presence of a U/A at the 3' cleavage site also enhances the kcat ten fold. Selected target regions were examined using the RNA folding algorithum designed by Micheal Zucker (REF) The folding program was used to fold 100-200 nucleotides on either side of the NUX cleavage site to determine whether the ribozyme binding location was acceptable. A BLAST search was also conducted to ensure the absence of target sites on any other known human or mouse mRNA sequence.

Preparation of Short Ribonucleic Acid Target

The target oligonucleotide to be used in the cleavage reactions was radioactively labeled at the 5'end using T4 polynucleotide kinase (New England Biochmeicals;

Beverly, MA). The reactions were set up as follows: 2µl of the RNA target oligo (10pmol/µl, 20pmol total)(Dharmacon, Boulder, CO) was added to a mixture containing 1ul of 10X polynucleotide kinase buffer (Promega, Madison, WI), 1ul RNASin (Promega, Madison, WI), 1ul 0.1M DTT (Sigma, St. Louis, MO), 3µl water, 1µl (gamma 32P) dATP (10uci) (ICN, Santa Clara CA) and 1µl of polynucleotide kinase (5 units) (Sigma, St. Louis, MO). The reaction was incubated at 37 °C for 30 minutes. 90µl of TE (Fisher, Swanee, GA) was added to the reaction prior to extraction of the unincorporated nucleotides. A spin column (1ml syringe) was prepared with sterile glass wool and loaded with sephadex (Sigma, St. Louis, MO) saturated in water. The column was centrifuged at 1000 RPM for 5 minutes to remove any excess water and to further pack the sephadex. The ^{32}P labeled target (100µl) was loaded on to the column. The column was sealed with parafilm and centrifuged again at 1000 RPM for 5 minutes. The labeled elute was collected in a 1.5ml Eppendorf tube (Fisher, Swanee, GA) and was stored at -20 °C.

Time Course Analysis

Time course analysis was done by setting up a cleavage reaction as follows: 13µl of 400mM Tris-HCL (Fisher, Swanee, GA), pH 7.4-7.5 were added to 1ul ribozyme (2pmol) (Dharmacon, Boulder, CO) and 88ul of water. In order to properly fold the ribozyme synthetic RNA, the above mixture was incubated at 65 °C for 2 minutes and then left at room temperature for 10 minutes. 13µl of a 1:10 ratio of RNasin: 0.1M DTT was added to the reaction mixture along with 13µl of 200mM $MgCl_2$ (20mM final) (Sigma, St. Louis, MO). The reaction was incubated at 37 °C for 10 minutes. 1µl of the 32P labeled (0.2 pmol) and 1µl of unlabeled target (20pmol total) were premixed and added to the reaction mixture at 37ºC. For each time point, 10 µl of the reaction mixture was removed from 37 °C and added to a tube containing 10ul of formamide dye mix

(90% formamide (Sigma, St. Louis, MO), 50mM ehtylenediamine tetra acetic acid (EDTA) pH 8 (Fisher,Swanee, GA), 0.05% bromophenol blue (Sigma, St. Louis, MO), and 0.05% xylene cyanol (Sigma, St. Louis, MO). The samples were initially placed on ice and then heat denatured at 90 °C for 3 minutes. The denatured samples were cooled on ice before loading 6 µl onto a 10% PAGE-8M urea gel to separate the products. Bromophenol blue band was run about 2/3 down the gel. The gels were analyzed on a molecular dynamics phosphoimager.

In Vitro Transcription of m-Htt mRNA

The human expanded *HD* transgene expressed in R6/1 mice was amplified from genomic DNA using the sense primer HDPCR1 (5'-agggctgtcaatcatgctggc-3') and antisense primer HDPCR1a (5'-tctgggttgctgggtcactctg-3'). This PCR fragment was cloned into the TOPO TA vector following manufacturer's protocol (Invitrogen, San Diego, CA). A HindIII / NotI fragment from the TOPO-R6/1 vector was cloned into the pRC/CMV (Invitrogen, San Diego, CA) plasmid in the forward orientation with respect to the cytomegalorivus immediate early promoter and a putative bacterial T7 promoter sequence. Radio-labeled transcripts were generated using Ambion's MAXIscript *In Vitro* Transcription Kit following manufacturer's instructions (Ambion, Austin, Tx). Transcripts were kept frozen at -20 ºC. Time course analysis was done with a ratio of ribozyme to transcript of 5:1. Reaction conditions were similar to those described above.

Cloning of Ribozymes into rAAV Vectors

Two complimentary DNA oligonucleotides (Invitrogen, San Diego, CA) were annealed in order to produce a double stranded DNA fragment coding for each hammerhead ribozyme. All DNA oligonucleotides were synthesized with 5'phosphate groups. The DNA oligonucleotides were designed to generate a cut HindIII site at the

5'end and a cut NsiI site at the 3' end after annealing. The DNA oligonucleotides were incubated at 90 °C for 2 minutes and annealed by slow cooling to room temperature for 30 minutes. The resulting double stranded DNA fragment was ligated into the HindIII and NsiI sites of the rAAV vector pTRUF-12 (UF vector Core, http://www.gtc.ufl.edu/gtc-home.htm). A self cleaving hairpin ribozyme has been cloned downstream of the inserted hammerhead ribozymes into a downstream ClaI site. Expression of the ribozyme cassette was placed under the control of the CMV, chicken-beta-actin chimeric enhancer-promoter. The ligated plasmids were transformed into SURE electroporation competent cells (Stratagene, La Jolla, CA) in order to maintain the integrity of the rAAV inverted terminal repeats. Ribozyme clones were sequenced in the University of Florida's DNA sequencing core (ICBR).

Human Embryonic Kidney 293 Cells

HEK 293 cells were obtained from American Type Culture Collection (ATCC) (Manassas, VA) and plated onto a 150 mm tissue culture dish. The cells were allowed to attach and grow to about 80% confluency. To ensure a homogenous population of HEK cells, the morphology of the HEK cells was recorded using a Zeiss microscope (Zeiss, Goettingen, Germany).

Transfections using Lipofectamine on HEK 293 Cells

HEK 293 cells were obtained from the American Type Culture Collection (ATCC) (Manassas, VA) and plated onto a 150 mm tissue culture dish. HEK 293 cells were fed with 1X high glucose Dubellco's modified Eagle medium (Invitrogen, San Diego, CA) containing 5 % fetal bovine serum (Invitrogen, San Diego, CA) twice weekly. The cells were cultured at about 80% confluency at which time they would be split on a 1:10 ratio. For transfection experiments, HEK 293 cells (ATCC, Manassas, VA) were seeded onto a

10-cm Corning™ tissue culture dish and allowed to attach and grow to 70-90% confluency. Lipofectamine™ and Plus™ reagents (Invitrogen, San Diego, CA) were used for the transient co-transfection of pCMV-R6/1 and rAAV-ribozyme expression vectors at a 1:5 or 1:10 pCMV-R6/1 to rAAV-ribozyme ratio. In order to control for transfection efficiency, 293 cells were also co-transfected with pCMV-R6/1 and a pTR-UF11 (rAAV-GFP) GFP vector at the same ratios. GFP expression was determined using a fluorescence microscope at 24hr and 48hr. Cells were harvested 48hr post-transfection

RNA Isolation and Northern Analysis

Total RNA was isolated from HEK 293 cells by using the TRIzol reagent (Invitrogen, San Diego, CA). Northern blot analysis was performed using standard techniques. Briefly, 25µg of total RNA were separated on a formaldehyde-containing 1.2 % agarose gel. Fractionated RNA was then transfer unto Hybond N+ membranes using alkalize transfer and probed with a ^{32}P product of a HindIII/AgeI digest of the pCMV-R6/1 vector (~ 150-bp of sequence spanning the 5'UTR and ATG translational start sites). Sample loading was normalized by stripping and re-probing the same membranes with a probe that recognizes nucleotides 150-270 of the human β-actin mRNA. Blots were exposed to phosphoimager-ready intensifying screens and intensity of bands was measured using a Phosphoimager scanner (Molecular Dynamics)

rAAV Vector Production

All rAAV vector preparations used in this study were made by the University of Florida Vector Core facility (Powell Gene Therapy Center). Briefly, rAAV vector is produced in human HEK 293 cells by transient CaPO4 precipitation-mediated co-transfection of the rAAV expression vector plasmid and a helper-plasmid that encodes the AAV rep and cap genes along with certain adenovirus genes (26). After 72 hours,

cells are harvested and stored at -80 ºC. Cell are resuspended in 0.5% sodium deoxycholate in 20 mM Tris, pH 8.0 and 150mM NaCl, treated with benzonase, and cellular membranes are disrupted by three cycles of repeated freeze-thaws. Crude lysates are purified using affinity chromatography, followed by cation exchange chromatography. The final product is concentrated to a final titer of 1-5 X 10^{13} genome copies per ml.

R6/1 Transgenic Colony

Animal experiments were performed in the laboratory of Eileen Denovan-Wright, PhD (Dept of Pharmacology, Dalhousie University, Halifax, Nova Scotia, Canada). Transgenic R6/1 HD mice were originally obtained from Jackson Laboratories and breeding colonies were maintained at Dalhousie University. R6/1 males were crossed with unrelated CBAxC57BL/6 females. After weaning, the mice were group housed under 12 h light-dark cycle with *ad libitum* access to food and water. All mice were genotyped at 3 weeks of age and at the time of death by amplifying a region of the human *huntingtin* transgene using primers 5' AGG GCGT GTC AAT CAT GCT GG 3' and 5' GGA CTT GAG GGA CTC GAA 3'. These primers correspond to a region upstream of the CAG repeat at nts 77-96 and 347-364, respectively, of human *huntingtin* (Genbank Accession number XM 003405). DNA was extracted from ear punches that were digested with Proteinase K and used as the substrate for PCR using the REDExtract-N-Amp Ready Mix (Sigma). Animal care and handling protocols were in accordance with the guidelines detailed by the Canadian Council on Animal Care and were approved by the Carleton Animal Care Committee at Dalhousie University.

Surgical Procedures

Isofluorane was delivered by inhalation to anesthetize the mice. After induction of anesthesia, the mice were placed into a sterotaxic frame (Kopf Instruments, Tujunga, CA). All injections were performed using a continuous infusion system (Carnegie Medicin, Sweden), attached to a 10 μl Hamilton microsyringe fitted with a glass micropipette with an outer diameter of 60-80 μm (Mandel *et al.*, 1999). The anterior-posterior (AP) and medial-lateral (ML) stereotaxic coordinates were calculated from bregma and the dorso-ventral (DV) coordinates were calculated from the dural surface. A burr hole was drilled in the skull at the calculated AP and ML coordinates. Mice received intrastriatal injections of rAAV2 or rAAV5 expressing HD6 or HD7 or GFP suspended in phosphate-buffered saline (PBS) at a dose of 2 μl/site and an infusion rate of 0.5 μl/min. During the infusion of rAAV, the glass pipette was slowly retracted 1 mm every min. One minute after the cessation of the infusion, the micropipette was retracted an additional 1 mm, allowed to remain at this position for 4 min and then slowly retracted from the brain. The stereotaxic coordinates used for two injections within the same striatum were: Site 1: AP = +1.0, ML = ± 1.8, DV = -3.3; Site 2: AP = +0.4, ML = $\pm$ 2.1, DV –3.4. The DV coordinate was calculated with the tooth bar set at 0.0 mm.

Tissue Processing

Ten-weeks after the intrastriatal infusion of rAAV, the mice were deeply anesthetized with sodium pentobarbital (65 mg/kg i.p.) and decapitated. The brains were removed and frozen at –70^{o}C. Tissue sections (14 μm) were cut using a Micron cryostat through the rostral-caudal axis of the striatum, thaw-mounted onto Fischer SuperFrost slides and stored at –70^{o}C**.** For each slide, 5 sections, each separated by approximately

350 μm, were placed on a single slide. This distribution of tissue was used to ensure that each slide contained sections taken throughout the anterior-posterior regions of the mouse striatum.

In Situ Hybridization Analysis

In situ hybridization was performed on coronal sections (Bregma +1.70 to –0.50; Franklin and Paxinos, 1997) of mouse brains using radiolabeled antisense gene-specific oligonucleotide probes. Frozen sections were allowed to reach room temperature, fixed with 4% paraformaldehyde in 1X phosphate-buffered saline (PBS) for 5 min, rinsed twice for 3 min in 1X PBS, once for 20 min in 2X sodium chloride-sodium citrate (SSC), and then air dried. Each slide was covered in 200 ul of hybridization buffer (50% deionized formamide, 5X SSC, 1X Denhardt's reagent, 0.02 M sodium phosphate, ph 6.8, 0.2% SDS, 5 mM Na2EDTA, 10 ug/ml Poly(A)n, 10% dextran sulfate, 50 ug/ml salmon sperm DNA, 50 ug/ml yeast tRNA) containing ~1 x 10^6 c.p.m./ml of oligonucletide probe that had been 3' end-labeled with [α-^{33}P]dATP for 90 min at 37^{o}C using terminal deoxynucleotidyl transferase (Promega). Prior to use, unincorporated nucleotides were removed from the labeled probes using a Sephadex G-25 spin column (Pharmacia). The slides were coverslipped with parafilm and incubated overnight at 42°C in a humidified chamber. The coverslips were removed in 2X SSC and the slides were washed for four times for 30 min at 55°C in 1X SSC, four times for 30 min at 55°C in 0.5X SSC, two times for 30 min at 55°C in 0.25X SSC, then rinsed briefly in H20 and allowed to air dry overnight. Slides were exposed to Kodak Biomax MR film for up to 4 weeks at room temperature. The hybridization signals were analyzed using Kodak 1D Image Analysis Software as described in Hebb et al. (2004). The sequences of the probes

used were: ribozyme probe (5'-cttacaccc cactcgtgcaggctgcccaggg-3'), ppEnk (5'tctgcatccttcttcatgaaaccgccatacctcttggcaaccat-3'), DARPP-32 (5'-tccacttggtcctcagagttgccatctctc-3'), NGF*i*-A (5'-ccgttgctcagcagcatgatgtc ctccagtttggggtagttgtcc-3'), D2 receptor (5'-ggcagggttggcaatgatacactcattctggtcttgatt-3'), β-actin (5'-ggcgatccacacggagtacttgcgctcaggaggagcaatgatct-3').

Results

Time Course of Ribozyme Cleavage

We initially screened ribozymes that were directed against four different regions along the mRNA sequence of the human HD transgene expressed in the R6/1 mouse. Figure 2-1A is a schematic of all four ribozymes and their target sequences. HD6 and HD7 ribozymes (Rbz) were targeted to unique and overlapping sequences that lie between the ATG translational start site and the polymorphic CAG repeat domain. dsCAG1 and dsCAG2 were targeted to unique sequences immediately downstream of the expanded CAG domain (Fig. 2-1B). Time course analysis of target cleavage was done for the HD6, HD7, dsCAG1 and dsCAG2 hammerhead ribozymes as described in the methods section. Figure 2-2 shows autoradiographs from 10% polyacrylamide-8M urea gels used to separate the products of cleavage of each of the four ribozymes and their targets following reactions performed at 37 °C and at 20mM $MgCl_2$. The autoradiographs show an increase in the 5'cleaved products over time and a corresponding decrease in the levels of target. Significant product accumulation was detected almost immediately after the addition of target to the reaction. Figure 2-2B shows a graphical representation of the percent of product cleaved as a function of time for all four ribozymes tested. This analysis demonstrated that HD6, HD7 and dsCAG1 could mediate the efficient cleavage

(~90% at the 10 minute time point) of target RNA *in vitro*. In contrast, dsCAG2 Rbz was unable to cleave more than 5% of its target after 60 minutes of reaction time.

HD6, HD7 and dsCAG1 Activity Against *In Vitro* Transcribed m-Htt mRNA

Success of ribozyme-mediated suppression of gene expression requires the identification of RNA target sites that are not masked by intrinsic RNA secondary structures. Although algorithms such as the M-fold program predict RNA secondary structure, determining the bio-availability of target sites requires an experimental approach. To examine the accessibility of target sites, we cloned the expanded human *HD* transgene that is expressed in the R6/1 mouse into a pRC/CMV (Invitrogen) expression vector (pCMV-R6/1). This vector can drive both in vitro and in vivo transcription of the cloned gene. We generated in vitro transcripts of the R6/1 transgene and performed cleavage reactions under identical conditions as described for the short-target time course cleavage reaction (see methods section). Figure 2-3A shows autoradiographs from 5% polyacrylamide gels used to separate the products of cleavage of both HD6 and HD7 Rbz following incubation with the R6/1 derived m-Htt transcript. Significant product accumulation from the HD7 Rbz reaction was initially detected 15 minutes after the addition of Rbz to target (Fig 2-3A, HD7 Rbz lane 1). There was an increase in the accumulation of the expected size product over time. In contrast, HD6 Rz mediated cleavage of m-Htt mRNA in vitro was not as efficient as the one observed with HD7 Rz (Fig 2-3). Nevertheless, the accumulation of product of the expected size suggests that this target site is available for binding and cleavage. In fact, as shown in figure 3-1B, HD6 and HD7 Rz have overlapping sequences. The small but significant

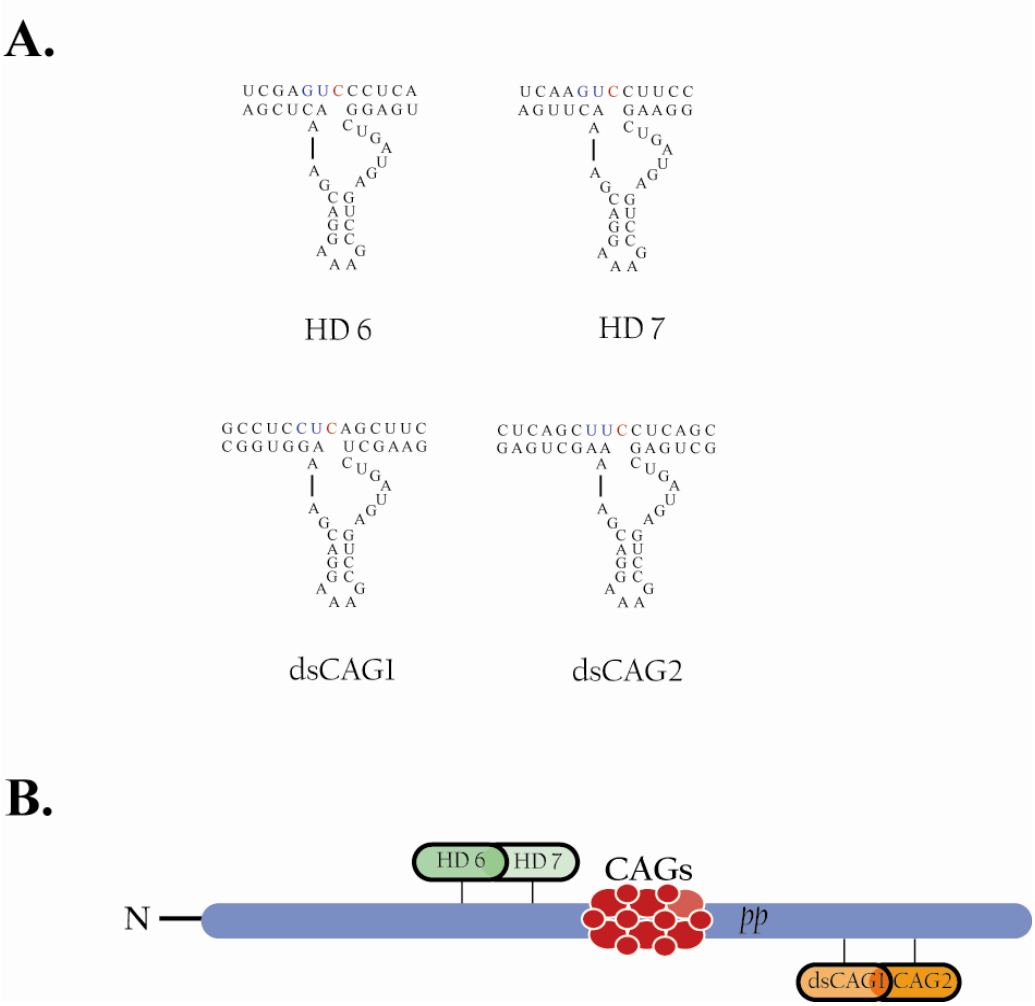

Figure 2-1. Ribozyme design. Four ribozymes were designed to target unique sequences in the human *HD* exon 1. In (A) ribozymes are shown annealing to their target sequences with the NUX triplet depicted in color. B. Illustration of the four target sites in relation to the CAG triplet repeat domain in human *HD* exon 1.

difference in turnover activity between these two Rbz might be explained by factors influencing the release of product. dsCAG1 Rbz was unable to mediate the cleavage of m-Htt transcript in vitro. This lack of enzymatic activity was likely due to the inability of dsCAG1 Rbz to properly bind to its target site within the context of m-Htt RNA's secondary structure.

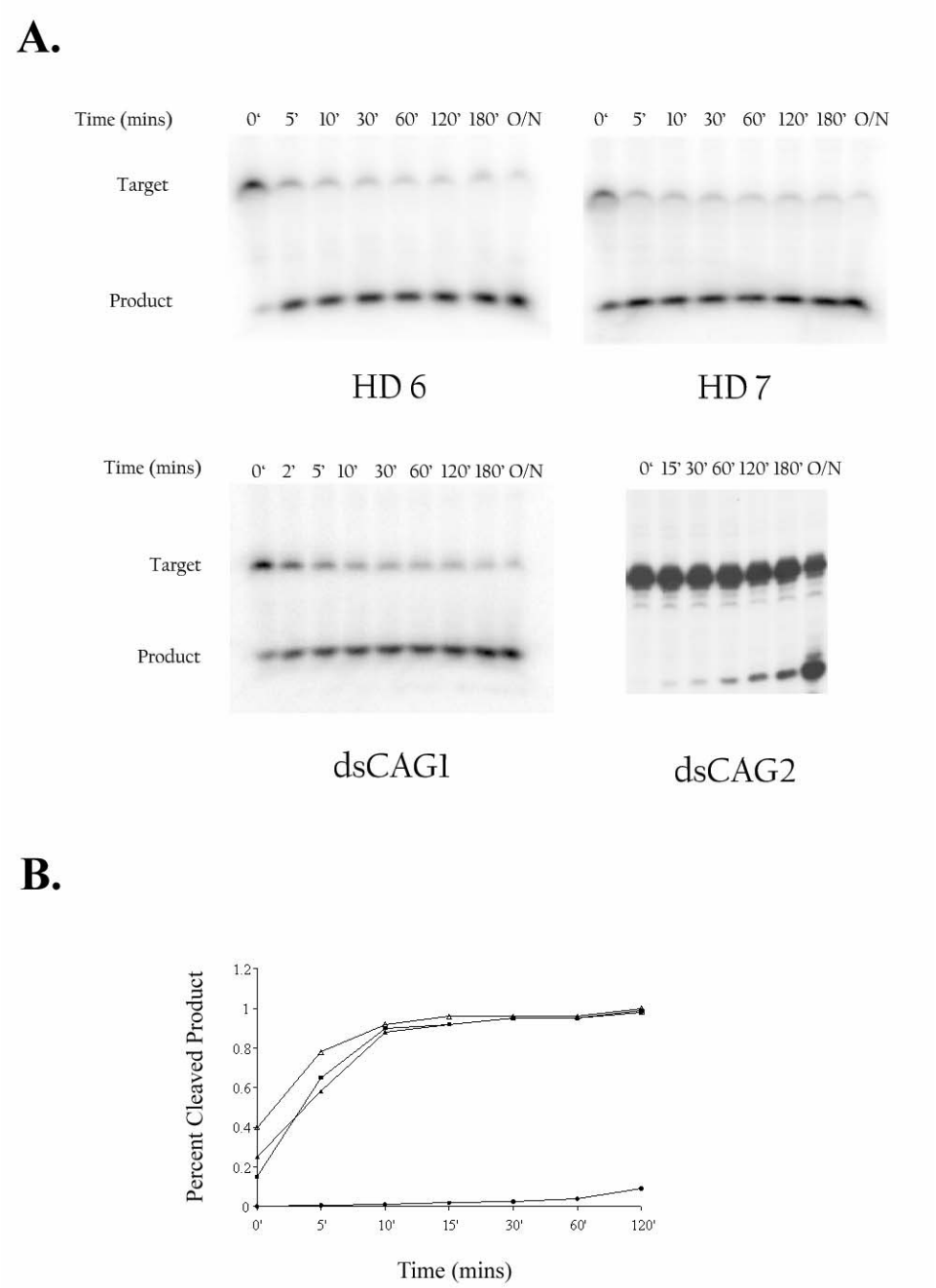

Figure 2-2. Time course cleavage analysis. A. Autoradiographs from 10% acrylamide gels used to separate the product of the reaction from the target. Target signal decreased while a corresponding product signal accumulated as a function of time. B. Graphical representation of the reactions shown above. Data is presented as percent target cleaved. Ribozymes HD6 (closed circles), HD7 (open triangles) and dsCAG1 (closed triangles) were capable of cleaving > 80% 10 mins into the reaction while dsCAG2 was much slower (closed circles).

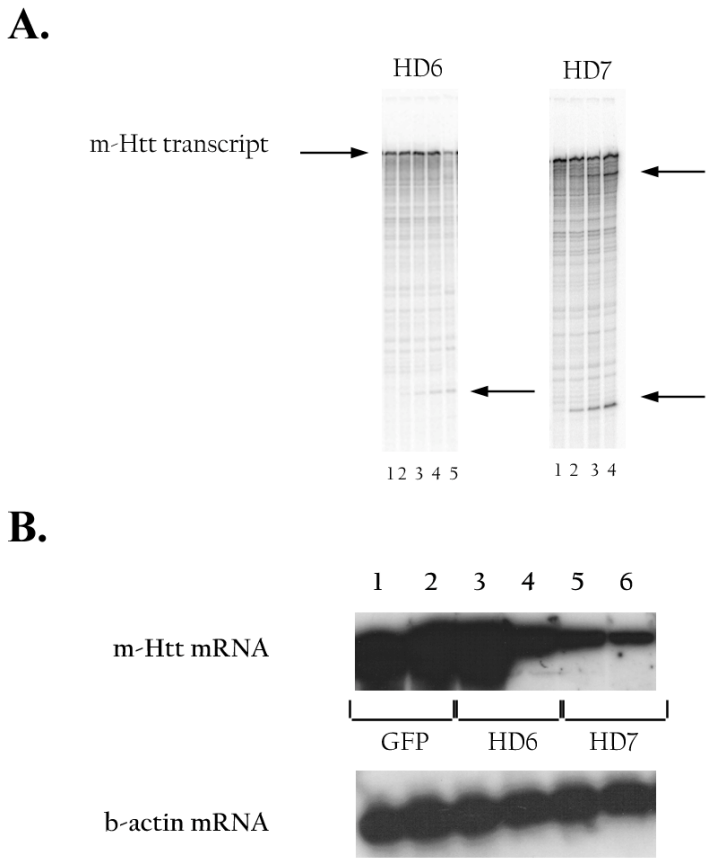

Figure 2-3. Target accessibility. A. Autoradiographs from 5 % acrylamide gels separating the products of a time course analysis of two highly active ribozymes, HD6, HD7. Both ribozymes were incubated with an *in vitro* transcribed human *HD* exon1 transcript (top left arrow) to determine the accessibility of the target sites within the context of a folded RNA molecule. Lanes 2-through-4 are the 15, 30, and 60 min time points for each reaction. Lane 1, in both autoradriographs, is a 60 min time point of a reaction that was devoid of ribozyme. Expected size products for both HD6 and HD7 accumulated over time (top and bottom right arrows). HD6 Rbz was less active against the *in vitro* transcribed human *HD* exon1 transcript (Lane 5 is an overnight incubation time point). Panel (B) is a northern blot analysis (top autoradiograph) of m-Htt mRNA. Total RNA was obtained from HEK 293 cells that were transiently co-transfected with pCMV-R6/1 (m-Htt) and either a GFP, HD6 or HD7 expression plasmid. Increasing the concentration of HD6 Rbz vector from a 1:5, target to ribozyme ratio (lane 3), to a 1:10, target to ribozyme ratio (lane 4), resulted in an increase in activity as determined by the intensity of the m-Htt mRNA band. HD7 Rbz activity against m-Htt mRNA

Figure 2-3 continued

remained constant at either 1:5 (lane 5) or 1:10 (lane 6) target to ribozyme ratio. The same blot was probed with a β-actin probe to normalize sample loading. Both ribozymes reduced m-Htt mRNA levels by > 60% when compared to controls.

HD6 and HD7 Ribozyme Activity Against m-Htt mRNA *In Vivo*

We next examined the activity of HD6 and HD7 Rbz against m-Htt mRNA in cultured HEK293 cells. HD6 and HD7 Rbz were cloned into a rAAV vector specifically engineered for the intracellular expression of HH Rbz (Figure 2-4A). This expression cassette generates a transcript that is processed by a self-cleaving hairpin ribozyme strategically placed downstream of the sequence encoding for either HD6 or HD7 Rbz. The self-cleaving activity of the hairpin ribozyme results in the release of a small HH Rbz-containing RNA and a transcript with an internal ribosomal entry site (IRES) sequence to facilitate the translation of the downstream GFP sequence.

In order to test the activity of these Rbz against m-Htt mRNA in culture, HEK293 cells were transiently co-transfected with CMV-R6/1 and either rAAV-HD6 or rAAV-HD7 Rbz vectors. Northern blot analysis of total RNA obtained forty-eight hours post-transfection showed a significant decrease (>60% of control) in the levels of m-Htt mRNA in samples obtained from both rAAV-HD6 and rAAV-HD7 transfected cells (Fig. 2-3B). This decrease was not evident in cells that were co-transfected with a rAAV-GFP expressing vector. Interestingly, increasing the rAAV-HD6 Rbz to target ratio from 1:5 to 1:10 resulted in a significant increase in cleavage activity (Fig 2-3B lanes 3 and 4).

***In vivo* Activity of rAAV-HD6 and rAAV-HD7 Ribozymes**

The focus of this study was to evaluate the effects that reduced striatal levels of m-Htt would have in the striatal-specific transcriptional dysregulation associated with the expression of m-Htt protein in the R6/1 mouse model of HD. Initially, we generated rAAV type 2 (rAAV2) particles encoding for HD6, HD7 or GFP control (see Methods). Intrastriatal injections of high-titer rAAV2 resulted in intense and localized transduction of the mouse striatum (Fig. 2-4B). Although the levels of viral expression attained with

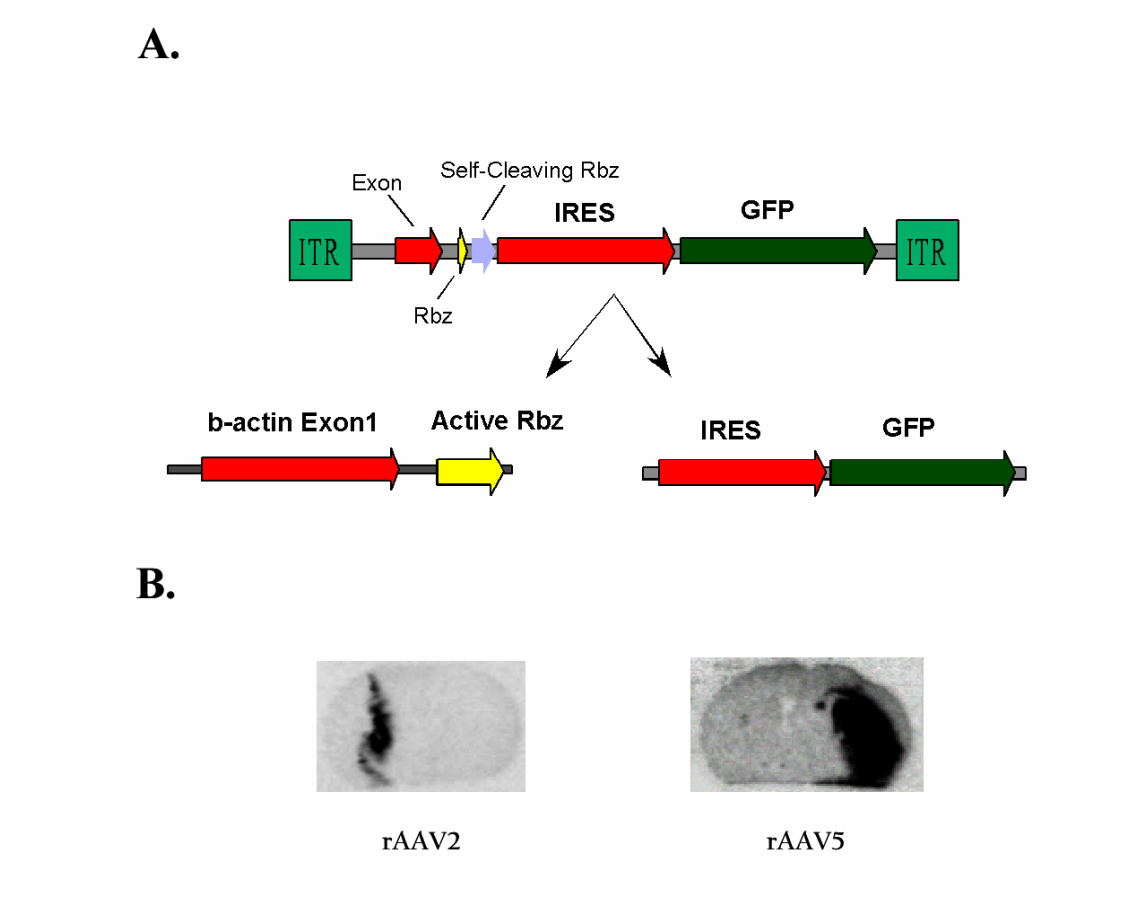

Figure 2-4. In vivo expression of rAAV ribozyme vectors. (A) Diagram depicting the ribozyme expression cassette that was packaged into rAAV viral particles. A hairpin self-cleaving ribozyme (self-cleaving Rz), placed immediately downstream from the HD6 and HD7 cloning sites, was used to mediate the processing of the primary Rbz-containing transcript. B. *In situ* hybridization analysis of the viral RNA transcript was done on coronal sections obtained from mice injected with either rAAV2 or rAAV5-HD7 vector. The ribozyme-specific probe was allowed to hybridize with the sections under identical conditions.

rAAV2 were remarkably high, the feasibility of this study was dependent upon extensive striatal transduction. We therefore generated rAAV viral vectors pseudotyped with the capsid from rAAV serotype-5 (rAAV5) encoding for HD6 (rAAV5-HD6 Rbz), HD7 (rAAV5-HD7 Rbz) and GFP (rAAV5- GFP). Our rationale was based on a recent elegant

study showing that intrastriatal delivery of rAAV5 particles in the rat brain results in a larger transduced area when compared to rAAV2 vectors (13). Intrastriatal delivery of rAAV5-HD6 or HD7 Rz in R6/1 and age-matched wild-type mice resulted in a dramatic increase in the brain transduced area when compared to rAAV2 particles as demonstrated by *in situ* hybridization (ISH) analysis using a Rbz-specific probe (Fig. 2-4B).

To determine the in vivo activity of rAAV5-HD6 and rAAV5-HD7, R6/1 and age-matched wild-type littermate controls were divided into the following experimental groups: rAAV5-HD6 (R6/1 n=8, wild-type n=5), rAAV5-HD7 (R6/1 n=8, wild-type n=5) and rAAV5-GFP (R6/1 n=5, wild-type n=5). Six week-old mice were injected unilaterally at two different striatal sites in the right hemisphere while the left hemisphere remained uninjected and served as control (Fig 2-4B). Ten weeks post-surgery fresh frozen brains were obtained, sectioned and maintained frozen throughout the remainder of the experiment.

Biological Effects of rAAV5-HD6 and HD7 Ribozyme Expression in the R6/1 Mouse Striatum

Alterations in gene transcription occur prior to the display of motor abnormalities in the R6/1 mouse of HD. Striatal-specific genes known to be downregulated in HD include the dopamine-, cAMP-regulated phosphoprotein of 32 kDa (DARPP-32), pre-pro-enkephalin (ppEnk), nerve growth factor-inducible A (NGFi-A) and the dopamine type-2 receptor (D2R).Reduction in the steady-state mRNA levels of these transcripts is both progressive and modulated by the length of the expansion repeat and the expression levels of m-Htt. Thus, ribozyme-mediated knockdown of m-Htt expression should lead to an increase in the transcript levels of ppEnk, DARPP-32, D2R and NGFi-A.

To test this hypothesis, we performed in situ hybridization analysis with probes specific to either NGFi-A, DARPP-32, ppEnk and D2R mRNAs (Fig 2-5). Analysis of coronal sections obtained from R6/1 mice unilaterally injected with rAAV5-HD6 or -HD7 ribozyme showed an unexpected sharp decrease in the mRNA levels of ppEnk, DARPP-32 and D2R around the area of transduction. Unexpectedly, expression of either rAAV5-HD6 or HD7 Rz exacerbated the rate of mRNA loss for most of the analyzed transcripts in the R6/1 mouse striatum (Fig 2-5A bottom panel). In contrast, there was a significant induction of NGFi-A mRNA in the right injected striatum of the R6/1 mouse. To further characterize this loss in mRNA steady-state levels, we analyzed sections obtained from injected age-matched wild-type mice. ISH analysis revealed a similar pattern of loss in transcriptional activity, albeit to a lesser degree (Fig. 3-5A top panel). This effect was specific to the intracellular expression of Rbz in striatal tissue since cultured HEK293 cells did not exhibit any HD6 or HD7 Rbz-associated toxicity. Furthermore, analysis of sections from rAAV5-GFP animals showed that long-term expression of rAAV5-GFP does not lead to detectable changes in the steady-state levels of either NGFi-A or D-32 mRNA (Fig. 2-5B).

We next investigated if this effect was associated with the expression of the self-cleaving hairpin ribozyme or the IRES-GFP transcript, which are encoded by our rAAV expression cassette (Fig. 2-4A). We injected wild-type mice with a rAAV2-HD7 Rz in the right hemisphere and rAAV2-hAAT Rz in the left hemisphere. hAAT Rz targets the human alpha-1 anti-trypsin (hAAT) liver enzyme which is not expressed in neuronal tissue. As shown by ISH analysis, rAAV2-HD7 Rz increased the steady-state levels of NGFi-A while causing a loss in the levels of D-32 mRNA (Fig. 2-5C).

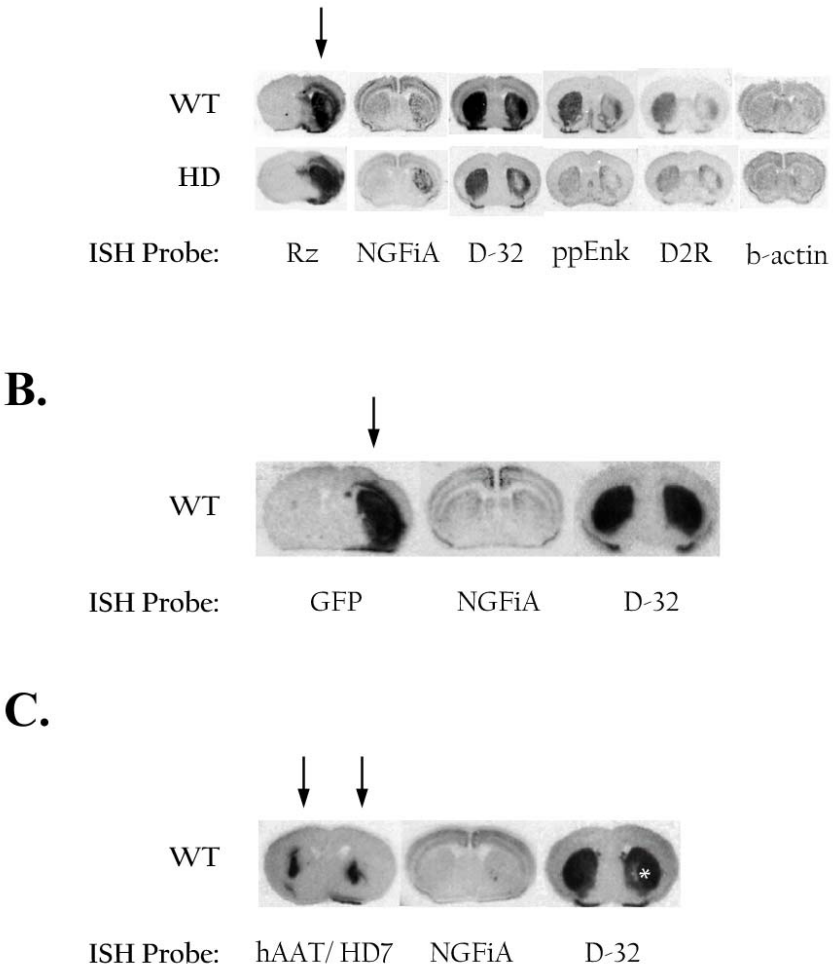

Figure 2-5. rAAV5-HD7 expression results in a loss of striatal-specific transcripts. A. *In situ* hybridization analysis of coronal sections obtained from a wild-type (WT) and a R6/1 (HD) mouse. Comparison between genotypes revealed a marked difference in the mRNA levels of NGF*i*-A, DARPP-32 (D-32), ppEnk and D2 receptor (left hemispheres). rAAV5-HD7 expression led to a remarkable loss in DARPP-32, ppEnk and D2 receptor mRNAs in both injected R6/1 and wild-type mice. In contrast, NGF*i*-A mRNA was increased to levels that were ~20% above wild-type in both wild-type and R6/1 injected mice. Panel (B) are coronal sections obtained from wild-type mice injected with a rAAV5-GFP vector. *In situ* hybridization analysis demonstrated that the loss in hybridization signal intensity of DARPP-32 and the increase in the levels of

Figure 2-5 continued

NGF*i*-A were specific to striatal expression of the HD7 ribozyme. C. Coronal sections obtained from wild-type animals expressing either rAAV2-HD7 ribozyme or a ribozyme targeting hAAT (rAAV2-hAAT). Analysis of DARPP-32 and NGF*i*-A expression revealed that the loss and gain in mRNA levels was specifically associated with the HD7 target sequence. Arrows on (A) and (C) denote the injected hemisphere.

Discussion

Ribozymes Can Modulate the Expression of Cellular Genes

There are a number of reports on the ability of the hammerhead ribozymes to control expression of specific genes in cell culture. For example, a hammerhead ribozyme designed to cleave mRNA encoding C-Ha Ras mutation inhibited formation of foci of transformed cells by 50% (22). Hammerhead ribozymes have also been used to target oncogenes. The use of hammerhead ribozymes targeted to survivin, which is expressed in carcinoma cells, resulted in up to 74% reduction in the levels of surviving mRNA (76). Finally, hammerhead ribozymes have also been shown to effectively reduce the levels of a rhodopsin mutant protein in vivo (34, 47). Taken together these data demonstrate that hammerhead ribozymes are capable of modulating the expression levels of targeted genes. This study demonstrates that hammerhead ribozymes can also be designed to suppress the expression of m-Htt in culture. However, upon detailed examination, our in vivo results showed an off-target effect associated with the expression of both HD6 and HD7 hammerhead ribozymes. This effect raises questions concerning the efficiency and safety of ribozymes as tools in molecular medicine.

In Vivo use of Ribozymes Directed Against the R6/1 Transgene

HD is a progressively devastating neurological disorder that currently affects the lives of approximately 30,000 individuals in the United States alone. Although pharmacological interventions exist that are designed to alleviate some of the excruciating symptoms associated with this disorder, HD remains largely without an effective treatment (53). The overall goal of this project was to develop a gene transfer strategy based on the rAAV-mediated delivery of anti-m-Htt hammerhead ribozymes in the striatum of the R6/1 mouse model of HD. This strategy was aimed at reducing the

levels of striatal m-Htt in order to prevent, reverse or ameliorate the symptoms associated with HD.

Four hammerhead ribozymes directed against the *HD* transgene expressed in the R6/1 mouse were designed and characterized *in vitro*. We showed that co-expression of either rAAV5-HD6 or HD7 Rbz with a m-Htt expression vector (pCMV-R6/1) results in significant reduction in the relative levels of m-Htt mRNA (> 60%) as determined by densitometric analysis. However, *in vivo* expression of rAAV5-HD6 or HD7 Rbz in the striatum of R6/1 mice resulted in a loss in the mRNA levels of striatal-specific genes known to be critical for neuronal function. This reduction in striatal mRNA levels was not due to a global suppression of transcriptional activity since the steady-state levels of the NGF*i*-A transcript were induced to levels that were ~20% that of control.

This result was unexpected and contrary to our initial hypothesis. Furthermore, *in situ* hybridization analysis of sections obtained from age-matched treated wild-type mice showed a reduction in the steady-state mRNA levels of the same striatal-specific genes. Since both of these ribozymes were directed against the human *HD* transgene in the R6/1 mouse and should not have cleaved any other known mouse RNA sequence, the loss of mRNA levels in wild-type animals lead us to conclude that there is an off-targeting effect associated with the striatal expression of HD6 or HD7 ribozymes which was not evident in cultured HEK293 cells. This off-targeting effect results in the cleavage of an unidentified RNA transcript that codes for a protein whose expression is necessary to neuronal function as evidenced by the loss of a subset of neuronal and striatal specific mRNAs in wild-type mice.

In an attempt to identify this transcript, we performed BLAST searches for short, nearly exact matching sequences. We limited the search, to sequences exhibiting greater than 50% sequence similarity to the HD6 and HD7 target site. Additionally, we only analyzed sequences that contained the required GUC triplet cleavage site and are expressed in neural tissue. Initial screens did not yield any significant matches to the human *HD* sequence spanned by the HD6 and HD7 target sites. However, the inclusion of expressed sequence tags (ESTs) during the search resulted in the identification of 6 sequences that have up to 60% similarity with the ribozymes target sites, contained the GUC triplet and are expressed in cultured neurospheres. The identification of the gene, or genes, responsible for the loss in striatal-specific mRNA levels might lead to the elucidation of an unknown gene function.

Conclusion

In this study we limited the designed of hammerhead ribozymes to sequences that are contained within the human *HD* transgene expressed in the R6/1 mouse. This transgene contains approximately 1 kb of 5'UTR sequence, an expanded exon 1 (117 CAG repeats) and 262 bases of intron 1. The design of ribozymes is limited by the NUX triplet rule where N is any nucleotide, U is uracil and X is any nucleotide but guanosine (Fig. 2-1). The small size of the transgene made the search for cleavage target sites extremely challenging. Furthermore, the identification of potential target sites does not necessarily correlate with the design of highly active hammerhead ribozymes as it was demonstrated in this study (Fig. 2-2A). These two factors limit our ability to test our underlying hypothesis using hammerhead ribozymes. Although the use of a full-length HD mouse model would increase the success probability of applying the use of hammerhead ribozymes to post-transcriptionally modulate the levels of m-Htt protein,

these models have slow, late-onset phenotypes that have not been fully described. Recently, the use of RNA*i* in a neurological model of disease led to cellular and behavioral improvements (91). This new technology is not dependent on NUX target rules and results in a more stable and long-term silencing effect. The application of RNA*i* in HD will be the focus in the next chapter.

CHAPTER 3
RNA INTERFERENCE OF MUTANT HUNTINGTIN IN VIVO

Introduction

The genesis and progression of disease in dominant genetic disorders, such as HD, require the presence and expression of a mutant allele. Nucleic acid-based molecules have been designed to inhibit gene expression by sequence-specific targeting of mutant mRNAs. It has been demonstrated that the expression of short, hairpin-like double-stranded RNA (shRNA) molecules in neuronal cells, both in vivo and in vitro, results in the sequence specific silencing of targeted genes (16). In fact, the successful in vitro application of synthetic siRNAs against members of the polyglutamine family of diseases, including HD, was recently reported (52, 57). This suppression was achieved by targeting siRNAs to either the CAG repeat region or to adjacent gene sequences and could even be designed to be allele-specific.

RNAi has also proven to be an efficient therapeutic tool in in vivo models of pQ disease. A recent report demonstrated the full potential of this technology in a transgenic mouse model of SCA-1 (91). In this experiment, cerebellar long-term expression of an anti-ataxin-1 siRNA was achieved by delivering an shRNA expression cassette with a recombinant adeno-associated viral vector. shRNA expression resulted in greater than 50% reduction of ataxin-1 protein in the cerebellum. Reduction in ataxin-1 transgene expression was associated with a rescue of the Purkinke cells as well as significant behavioral improvements in this model of SCA-1. This elegant study, addressing the applicability of RNAi in neurological disease, suggests that the pathological mechanism

associated with HD could be effectively halted or reversed by introducing siRNAs that can target the striatal expression of mutant Htt.

In this study, we examined the effects of RNAi mediated post-transcriptional silencing of striatal m-Htt in the R6/1 mouse. We specifically assessed whether reduced levels of striatal m-Htt could affect the transcriptional dysregulation phenotype that is associated with the expression of m-Htt in the R6/1 mouse striatum. Long-term in vivo expression of two rAAV5-shRNA vectors lead to the significant reduction in striatal m-Htt mRNA and protein levels as determined by real-time quantitative RT-PCR, western blot and immunohistochemistry analysis. This reduction was concomitant with a decrease in both the size and number of neuronal intranuclear inclusions (NIIs). Finally, reduced levels of striatal m-Htt resulted in an increase in the steady-state levels of ppEnk and DARPP-32 transcripts as well as in mild-behavioral improvements.

Materials and Methods

rAAV-shRNA Plasmid Construction

Two complimentary DNA oligonucleotides (Invitrogen, San Diego, CA) were allowed to anneal in order to produce a double-stranded DNA fragment coding for the sense strand, 9 nucleotide loop and antisense strand of both anti-huntingtin shRNAs tested. siHUNT-1 targeted nucleotides 262-281 (5'-GCCGCGAGTCGGCCCGAGGC-3', Fig. 3-1B) and siHUNT-2 targeted nucleotides 342-363 (5'-GGCCTTCGAGTCCCTCAAGTCC-3', Fig. 3-1B) of the human HD mRNA (Genbank accession no. L12392). Double-stranded DNA fragments were ligated into the *Bgl*2/*Hind*III sites of the rAAV vector pSOFF-H1p-hrGFP. This vector contains the human RNAse P H1 promoter downstream of the rAAV serotype-5 ITR and a cDNA

encoding the humanized *Renilla reniformis* GFP (Stratagene, La Jolla, CA) protein under the control of the herpes simplex virus thymidine kinase (HSV-TK) promoter.

Testing of shRNA Efficacy in Cultured Cells

A portion of the *mHtt* transgene was PCR amplified from R6/1 mouse genomic DNA using forward (5'-AGGGCTGTCAATCATGCTGG-3') and reverse (5'-TCTGGGTTGCTGGGTCACTCTGTCTCTGCGGAGCCGGGGG-3') primers. The resulting product was cloned into pCR 2.1-TOPO TA cloning kit (Invitrogen, Carlsbad, CA), sequenced and subcloned into the *Hind*III/*Nsi*I sites present in the pRC/CMV (Invitrogen, Carlsbad, CA) eukaryotic expression plasmid. The resultant plasmid (pCMV-R6/1) expressed part of the 5'UTR, the coding region within exon 1 with ~115 contiguous CAG repeats, and part of intron 1 of the *mHtt* transgene under the control of the minimal cytomegalovirus (CMV) promoter.

Human embryonic kidney 293T (HEK293) cells (ATCC, Manassas, VA) were seeded onto a 10-cm Corning™ tissue culture dish and allowed to attach and grow to 70-90% confluency. Lipofectamine™ and Plus™ reagents (Invitrogen, San Diego, CA) were used for transient co-transfection of HEK293 cells with pCMV-R6/1 and rAAV-shRNA vectors at a ratio of 1:4 and 1:8 respectively. In order to control for non-specific off-targeting effects, we performed co-transfection of the pCMV-R6/1 plasmid with a rAAV-shRNA vector targeting the dog rhodopsin mRNA (siRho-1). rAAV-siRho-1 has been shown to be active against its target both *in vitro* and *in vivo* (M. Gorbatyuk and A. Lewin manuscript submitted). Transfection efficiency was determined by analysis of GFP-positive cells and ranged from 70-80%. All transfected cells were harvested 48 hr post-transfection for northern and western analysis. Total RNA was isolated from transfected HEK293 cells using TRIzol™ reagent (Invitrogen, San Diego, CA). Northern

blot analysis was performed using standard techniques ("Current Protocols in Mol Biol, Wiley editing house). Briefly, 10 μg of total RNA was fractionated on a 1.2 % formaldehyde agarose gel and transferred to Hybond N+ (Amersham, Piscataway, NJ) membrane by capillary action. pCMV-R6/1 was subjected to restriction enzyme digestion using *Hind*III and *Age*I, the 150 bp fragment spanning the 5' UTR and ATG initiation codon of the *mHtt* transgene was gel-purified, radio-labeled using [α-^{32}P]dCTP (3000 mCi/ml; MP Biochemicals, Irvine, CA) and used as the hybridization probe. RNA loading was normalized by removing the *mHtt*-specific probe and re-probing the membrane with a radio-labeled fragment complementary to nucleotides 150-270 of the human β-actin mRNA (Genbank accession no. BC002409). Blots were exposed to phosphoimager-ready intensifying screens and the intensity of labeled bands was determined using a Molecular Dynamics phosphoimager.

Western Blot Analysis using Hum-1 Antibody

A polyclonal antibody (Hum-1) was raised in New Zealand white rabbits against the human Htt-synthetic peptide Ac-PQLPQPPPQAQPLLPQPQC-OH and affinity-purified (New England Peptide, Gardner, Massachusetts). Pre-immune serum was used as a control. Western blot analysis was performed by blocking the membranes for 2 hr at room temperature in 5% (w/v) skim milk powder in 20 mM Tris, 146 mM NaCl, 0.1% Tween-20 (TBST), incubating the membranes in a 1:500 dilution of affinity-purified polyclonal rabbit anti-human huntingtin transgene protein (Hum 1) antibody in 5% (w/v) skim milk powder/TBST at 4º C overnight. Membranes were washed 2 x 20 min in TBST. A peroxidase-labeled goat anti-rabbit IgG secondary antibody (1:2000, Vector Laboratories, Burlingame, CA) was incubated for 1 hr at room temperature in 5% skim

milk powder/TBST. Interaction between the primary and secondary antibodies was detected using West Pico SuperSignal® chemiluminescent substrate using the protocol recommended by the manufacturer (Pierce Biotechnology, Rockford, IL) and Hyperfilm ECLTM (Amersham Pharmacia Biotech, England)

rAAV Vector Production

All rAAV vector preparations used in this study were produced by the University of Florida Powell Gene Therapy CenterVector Core facility using the method described in [47]. The rAAV5 vector used in this study consisted of rAAV5 capsids and AAV5 ITRs and is therefore not a pseudotyped vector (13). A standard triple transfection method using the helper DNAs pDG [49] for required adenoviral proteins, our transgene plasmid described above and pAAV5.2 which has *rep* and *cap* from AAV5. Crude rAAV5 virus was then purified by iodixanol step gradients and Sepharose Q column chromatography as previously described (13). The final product is concentrated to final titers of 1 to 5 X 10^{13} genome copies per ml.

Intrastriatal Injection of shRNA-Expressing AAV Vectors.

All animal care, handling and surgical protocols were in accordance with the guidelines established by the Canadian Council on Animal Care and were approved by the Carleton Animal Care Committee at Dalhousie University. Transgenic R6/1 HD mice were obtained from Jackson Laboratories and used to establish a breeding colony at Dalhousie University. R6/1 males were crossed with unrelated CBAxC57BL/6 females. After weaning, the mice were group housed under a 12 h light-dark cycle with *ad libitum* access to food and water. All mice were genotyped at 3 weeks of age and at the time of death by amplifying a region of the human *HD* transgene as described previously (36).

Stereotaxic administration of AAV vectors were performed on 6 to 8 week-old wild-type and R6/1 mice under isofluorance anesthesia. The anterior-posterior (AP) and medial-lateral (ML) stereotaxic coordinates for injection were calculated from bregma and the dorso-ventral (DV) coordinates were calculated from the dural surface. Mice received intrastriatal injections of rAAV5 expressing siHUNT-1, siHUNT-2 or TRUF11 (rAAV5-hrGFP) suspended in phosphate-buffered saline (PBS) at a dose of 2 μl/site and an infusion rate of 0.5 μl/min using a continuous infusion pump, attached to a 10 μl Hamilton microsyringe fitted with a glass micropipette with an outer diameter of 60-80 μm. One minute after the cessation of the infusion, the micropipette was retracted an additional 1 mm, allowed to remain at this position for 4 min and then slowly retracted from the brain. The stereotaxic coordinates used for the two injections within the same striatum were: Site 1: AP = +1.0, ML = ± 1.8, DV = -3.3; Site 2: AP = +0.4, ML = ± 2.1, DV –3.4 (All coordinates were measured with an empirically determined flat skull).

The effect of shRNA and control vectors on mHtt mRNA and protein levels was assessed in a group of animals that received unilateral intrastriatal injections of rAAV vectors. In these experiments, the contralateral hemisphere was used as an internal control. Ten-weeks after the intrastriatal infusion of rAAV, mice were deeply anesthetized with sodium pentobarbital (65 mg/kg i.p.) and decapitated. The brains were removed and stored at –70oC. Tissue sections (14 μm) were cut using a Micron cryostat through the rostral-caudal axis of the striatum, thaw-mounted onto Fisher SuperFrost™ slides and stored at –70oC. For each animal, 5 coronal brain sections, each separated by approximately 350 μm, were placed on a single slide. This distribution of tissue was used

to ensure that each slide contained sections taken throughout the transduced region of the striatum.

To determine the levels of mHtt RNA and protein, striatal tissue was isolated from frozen sections that had been thaw-mounted on slides. Cortical tissue was removed using a razor blade and discarded. To collect tissue mainly from the transduction area, sections were first examined under epi-fluorescence to visualize the transduction area. The striatal tissue from the right and left sides of 5 brain sections per animal were then manually scraped from each slide taking only the approximate area of GFP positivity.

RNA was extracted using Trizol ™ (Invitrogen, San Diego, CA), quantified spectrophotometrically and used as the substrate for reverse-transcriptase (RT) reactions to generate single-stranded cDNA. The reaction was optimized to reverse transcribe the 5' end of the human *Htt* transgene. Briefly, 1 μg of total RNA and 0.75 μg of random hexamers were incubated with 1 μl of 5X Q solution (Qiagen, Valencia, CA) in a total volume of 5.75 μl at 70^{o}C for 3 min, mixed and placed on ice for 5 min. M-MLV RT buffer and dNTPs were added to a final concentration of 1X and 1.25 μM, respectively, in a final reaction volume of 10 μl. 20 Units of RNasin (Promega, Madison, WI) and 100 Units of M-MLV RT (Promega, Madison, WI) were added and the reaction was allowed to proceed at 48^{o}C for 60 min. The reaction was terminated by heating at 70^{o}C for 10 min. –RT reactions differed from +RT reactions by the substitution of H_20 for RT in the reactions. Quantitative PCR (Lightcycler, Roche) was used to amplify a 115 bp region of mHtt cDNA from striatal tissue. The PCR reactions contained 1X QuantiTect SYBR Green PCR master mix (Qiagen), 500 nM each of sense (5'-AGAGCCCCATTCATTGCC- 3') and antisense (5'-GGACTTGAGGGACTCGAA-3')

primer. Cycling conditions included a denaturation step of 95°C for 15 min, followed by 45 cycles of 94°C for 15 s, 58°C for 20 s, and 72°C for 20 s, and ending with a melting step from 65°C to 99°C over 30 s. Total SYBR green fluorescence was measured at the end of each PCR cycle and continuously through the melting step. Known quantities of mHtt cDNA were simultaneously amplified with experimental samples and used to create a standard curve. The levels of cDNA in each sample were normalized to the levels of hypoxanthine ribosyl transferase.

For western blot analysis, striatal tissue from 4-5 sections per animal were isolated and homogenized in 0.32 M sucrose, quantified using the BCA protein determination assay (Pierce), fractionated on SDS/PAGE gels using standard protocols and subjected to the immunoblotting conditions described for analysis of mHtt protein levels in transiently transfected HEK293 cells.

For analysis of the distribution of immunoreactive inclusion bodies, fresh-frozen coronal brain sections on SuperFrost slides were allowed to come to room temperature, rinsed 3 x 10 min with phosphate-buffered saline (PBS: 100 mM phosphate, pH 7.4, and 0.9% NaCl) and the tissue was fixed in 4% (v/v) parafomaldehyde for 15 min. The tissue was incubated in 0.1% (v/v) H_2O_2, 10% methanol and PBS for 10 min and rinsed 3 x 10 min in PBS. Non-specific binding sites were blocked in a solution of 5% normal goat serum in 0.25% (v/v) Triton-X100/0.01 M PBS for 1 hr at room temperature. Immunostaining was performed using a 1:500 dilution of affinity-purified Hum 1 or 1:4000 dilution of polyclonal rabbit anti-ubiquitin (IgG) antibody (DakoCytomation, Carpinteria, CA) in 1% (v/v) normal goat serum, 0.25% (v/v) Triton-X100/ PBS. Tissues were incubated overnight at 4º C. A 1:500 dilution of goat anti-rabbit biotin-labeled

secondary antibody (Vector, Burlingame, CA) was prepared in 1% (v/v) normal goat serum, 0.25% (v/v) Triton-X100/0.01 M PBS. Slides were incubated in secondary antibody solution for 2 hr at room temperature then rinsed 3 x 10 min in 0.01 M PBS. Interaction between the primary and secondary antibodies was detected using the Vectastain Elite ABC Kit (Vector, Burlingame, CA) and DAB using the company's standard protocol.

The size and distribution of Hum-1 immunoreactive NIIs were determined by using the *Analyze Particle* function in the Image *J* NIH software (freeware available at http://rsb.info.nih.gov/ij/). Briefly, the relative size (μm^2) and amount of NIIs were determined by analyzing coded digital images of four different regions (left motor cortex, right motor cortex, left medial striatum, right medial striatum) in coronal sections that were subjected to the stringent immunohistochemical procedure described above. Fourteen μm sections were too thin for unbiased stereological estimates of NII number and the NIIs diameter was too small to use the rotator method of volume estimation [53]. The Image *J* software (NIH) was configured to detect particles of a specified size range (0.03 μm^2-0.5 μm^2) and a constant upper and lower threshold value was used for all grayscale images from all areas analyzed. The mean relative size area (μm^2) of particles (NIIs) as well as the mean number of particle counts within the specified size range was calculated by a blinded operator for each of the four different regions in all of the unilaterally injected R6/1 mice and reported as percent of the size and number of NIIs present in the left motor cortex. Since absolute numbers or areas are not reported and internal section controls were used to determine percent controls, this method of quantification of NIIs is valid.

In Situ Hybridization Analysis

In situ hybridization was performed on coronal mouse brain sections (Bregma +1.70 to –0.50) using radio-labeled antisense gene-specific oligonucleotide probes (Table 1). Frozen sections were allowed to reach room temperature, fixed with 4% paraformaldehyde in 1X PBS PBS for 5 min, rinsed twice for 3 min in 1X PBS, once for 20 min in 2X sodium chloride-sodium citrate (SSC, 0.15 M NaCl, 0.015M NaCitrate, pH 7.4), and then air dried. Each slide was covered in 200 μl of hybridization buffer (50% deionized formamide, 5X SSC, 1X Denhardt's reagent, 0.02 M sodium phosphate (pH 6.8), 0.2% SDS, 5 mM Na2EDTA, 10 μg/ml Poly(A)n, 10% dextran sulfate, 50 μg/ml sheared salmon sperm DNA, 50 μg/ml yeast tRNA) containing ~1 x 106 c.p.m./ml of oligonucletide probe that had been 3' end-labeled with [α-33P]dATP (2000 mCi/ml) for 90 min at 37oC using terminal deoxynucleotidyl transferase (Promega, Madison, WI). Prior to use, unincorporated nucleotides were removed from the labeled probes using a Sephadex G-25 spin column (Amersham Biosciences, Buckinghamshire, UK). The slides were coverslipped with parafilm and incubated overnight at 42oC in a humidified chamber. The coverslips were removed in 2X SSC and the slides were washed for four times for 30 min at 55oC in 1X SSC, four times for 30 min at 55oC in 0.5X SSC, two times for 30 min at 55oC in 0.25X SSC, then rinsed briefly in H20 and allowed to air dry overnight. Slides were exposed to Kodak Biomax MR film for up to 4 weeks at room temperature. The hybridization signals were analyzed using Kodak 1D Image Analysis Software as described in (36).

For display purposes in order to make differences in hybridization signal easier to visualize, hybridized sections were scanned and false-colored in Adobe Photoshop ™ 7.0

by changing the image to RGB color and then a gradient map (as shown at the bottom of Fig. 3-5) was applied. This was done to all coronal sections shown in figure 3-5 without any further manipulation.

Effect of Anti-mHtt shRNA on Phenotype

The effect of anti-mHtt shRNA and control vectors on phenotype were assessed in animals that received bilateral injectons of siHUNT-1, siHUNT-2 and control rAAV vectors. Mice were weighed weekly following injection of rAAV. Average weight, grouped by genotype and treatment, was determined for each week, and significant differences determined using ANOVA Hind limb clasping behavior was assessed by suspending the mice 30 cm above a flat surface by their tail for 60 seconds or until the mice curled and clasped their hind limbs with their forelimbs and maintained the posture. The percentage of mice per group at each time point that exhibited clasping was recorded. Motor coordination was analyzed by placing the mice on rotarod that increased from 0 to 40 rpm over 1 min. The time from placing the mouse on the rotarod until the mouse fell off was recorded for each of 4 trials and the average time that each mouse remained on the rotarod was recorded.

Statistics

Analysis of variance (ANOVA) was used to evaluate the probability of differences between experimental groups. Where appropriate, one-way ANOVA was performed and individual *post-hoc* differences between groups was assessed using Fisher's paired-least-significant-difference test (Fisher's PLSD as available in Statview). Post-hoc differences in two-way ANOVA designs were assessed in a hierarchical fashion as described by Kirk et al (8) using simple main-effects analysis. The minimum probability accepted for significance (α level) was 0.05.

Results

RNA Interference of Mutant Huntingtin In Vitro

R6/1 trangenic HD mice express exon 1 of human *Htt* with ≈115 CAG repeats [14]. We designed short-hairpin RNAs (shRNA) (20 to 21 nucleotides in length) that could target specific sequences of exon 1 of human Htt, but did not have significant sequence similarity to the endogenous mouse Htt mRNA. We generated rAAV5-based DNA constructs expressing two anti-mHtt shRNA molecules (Fig. 3-1A). The mHtt silencing activity of these constructs was tested *in vitro* by transiently co-transfecting each construct with a eukaryotic expression vector containing the R6/1 *HD* transgene (*mHtt*) into HEK293 cells. Transfections were performed using a 1:4 and a 1:8 target vector to shRNA vector ratio. Forty-eight hours post-transfection, we analyzed mHtt mRNA and protein expression levels. Northern blot analysis of total RNA obtained from HEK293 cells co-transfected with a shRNA vector targeting nucleotides in the 5'-UTR of the mHtt mRNA (siHUNT-1) or a shRNA vector targeting a region immediately upstream of the CAG repeat domain (siHUNT-2) resulted in greater than 75% ($p < 0.001$) reduction of mHtt mRNA compared to samples from cells that expressed mHtt and a GFP-only vector (Fig. 3-1B). Co-transfection with a control shRNA vector targeted to the dog rhodopsin mRNA (siRho-1) did not affect the levels of mHtt mRNA (Fig. 3-1B).

Immunoblot analysis of mHtt protein using a human amino-terminus specific Htt antibody (Hum-1) showed that the reduction in mRNA levels was associated with a significant decline in the levels of mHtt protein (Fig. 3-1C). Co-expression of the mHtt vector with siHUNT-1 shRNA reduced the levels of mHtt protein to ≈ 40% ($p < 0.001$) of that observed in cells co-transfected with either a GFP-only vector or the siRho-1 shRNA control vector. We also observed ≈55% ($p < 0.001$) reduction in the levels of mHtt

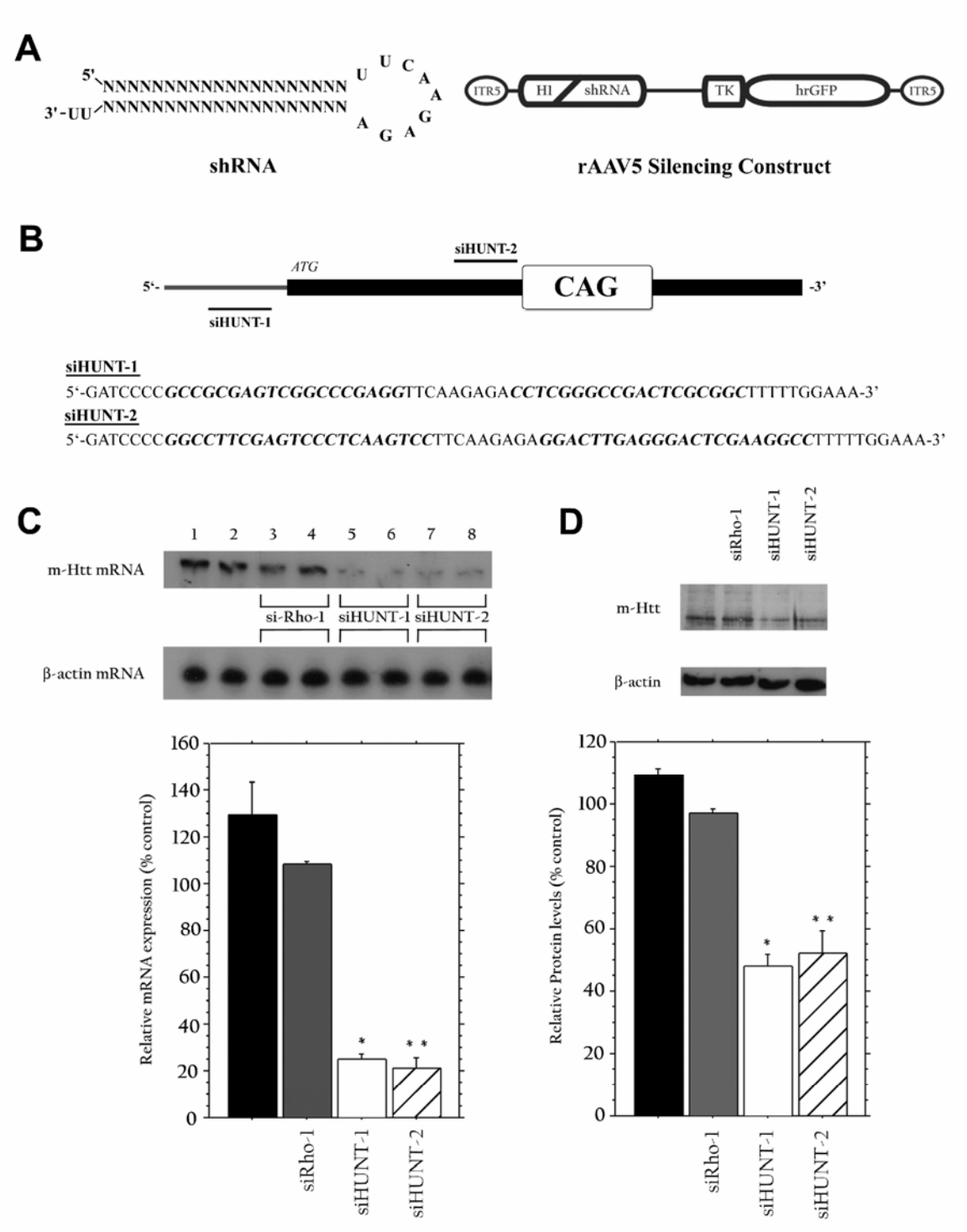

Figure 3-1. rAAV-shRNA constructs mediate the silencing of m-Htt in vitro. A. The human H1 RNA promoter unit was used to drive the intracellular expression of 20 to 21-nucleotide long shRNAs directed against the R6/1 *HD* transgene (mHtt) from within the context of rAAV serotype-5 vectors. Expression of hrGFP was used to positively identify transduced cells. B. Schematic

Figure 3-1 continued

representation of the *Htt* gene graphically showing the region of the gene that is targeted by siHunt-1 and siHunt-2 shRNAs. C. Northern blot analysis of mHtt mRNA obtained from transiently co-transfected HEK293 cells. Co-expression of CMV-R6/1 (mHtt) with either siHUNT-1 or siHUNT-2 shRNA constructs, at either a 1:4 (lane 5 and 7) or 1:8 (lane 6 and 8) target to shRNA ratio, resulted in significantly reduced levels of mHtt mRNA when compared to co-transfection with a control shRNA, siRho-1, (lanes 3 and 4) or CMV-R6/1 alone (lanes 1 and 2). Comparisons of the average optical density signal from three independent experiments performed with a 1:8 target to shRNA ratio showed greater than 75% reduction in mHtt mRNA relative to levels of β-actin mRNA (* = $p<0.001$, ** = $p<0.001$). D. Western blot analysis of total protein from HEK293 cells treated as above. mHtt protein was detected using a human-specific anti-Htt antibody (Hum-1). Analysis of the average (+ SEM) optical density signal revealed that mHtt was silenced by intracellular expression of both siHUNT-1 (>60% reduction, * = $p<0.0001$) and siHUNT-2 (>55% reduction, ** = $p<0.0001$). Silencing of mHtt protein expression was not observed in cells co-transfected with siRho-1. The same blot was probed with an antibody to β-actin in order to normalize for total protein load. Error bars represent + standard error of the mean (+SEM).

protein in samples from cells transfected with siHUNT-2 shRNA. mHtt protein levels were unaffected by the expression of siRho-1 shRNA molecules (Fig. 3-1C). These *in vitro* results demonstrate that intracellular expression of both siHUNT-1 and siHUNT-2 results in the specific and efficient knockdown of mHtt mRNA and protein levels in cultured HEK293 cells.

Long-Term Striatal Expression of rAAV5-shRNAs in the R6/1 Mouse

We next investigated whether rAAV5-mediated long-term striatal expression of siHUNT-1 or siHUNT-2 shRNAs could induce RNA interference of the mHtt transgene in the R6/1 transgenic HD mouse. To test the in vivo activity of both shRNAs, 6-8 week old R6/1 mice and wild-type littermates were divided into four groups and injected unilaterally at two different sites in the right striatum. Each intrastriatal injection delivered 2 µl of high-titer rAAV5-siHUNT-1 (R6/1 n=12, wild-type n=6), rAAV5-siHUNT-2 (R6/1 n=13, wild-type n=5), rAAV5-siRho-1 (R6/1 n=4) or rAAV5-GFP (R6/1 n=5, wild-type n=5) viral vectors. Ten weeks post-surgery, fresh-frozen coronal brain sections were obtained and viral transduction, mHtt mRNA levels, and protein expression levels relative to the left untreated hemisphere were determined.

Injection of rAAV5-GFP, rAAV5-siRho-1 and anti-mHtt rAAV5 shRNA vectors resulted in widespread and intense neuronal transduction as was previously observed in the rat striatum (13). *In situ* hybridization (ISH) analysis performed on coronal sections against the rAAV5-encoded hrGFP mRNA revealed a non-uniform but widespread rAAV5 transduction (Fig. 3-3A). hrGFP mRNA was efficiently expressed along the dorsal-ventral and rostral-caudal axis of the striatum. A strong hybridization signal was detected on either side of the corpus callosum but not in the white matter tracts (Fig. 3-3A) suggesting that the majority of hrGFP signal was concentrated in neuronal cell

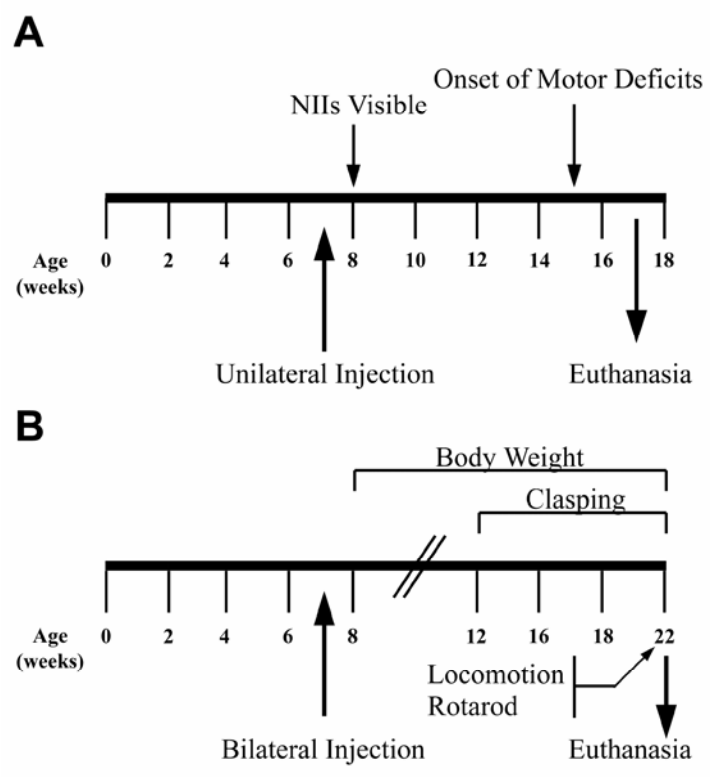

Figure 3-2. Experimental design. A**.** R6/1 and littermate control animals were injected unilaterally with either rAAV5-siHUNT-1, -siHUNT-2, -siRho-1 or -GFP viral vectors (annotated below the line). B**.** Experimental design for bilateral injections was identical to that shown above. Behavioral tests were performed weekly between the time points indicated by the arrows above and below the time-line.

bodies. hrGFP protein expression was intense and paralleled the widespread pattern of rAAV5 transduction detected by ISH analysis (Fig. 3-3B). Native hrGFP epiflourescene was observed in all sections that contained rAAV5-transduced striatal tissue such as the one shown in figure 3-3B. Long-term striatal expression of control rAAV5 vectors (rAAV5-siRho-1, rAAV5-GFP) in the R6/1 mouse was not associated with any abnormal changes in cellular morphology or astrocyte activation as determined by cresyl violet and GFAP staining (data not shown). These observations demonstrated that the striatum of

the R6/1 mouse can tolerate strong, wide-spread and long-term rAAV5-mediated expression of hrGFP and shRNA molecules.

To evaluate the silencing activity of rAAV5-siHUNT-1 and rAAV5-siHUNT-2 *in vivo*, we extracted total cellular RNA from rAAV5-shRNA-transduced striatal regions and subjected the RNA to reverse-transcription reactions optimized to convert the GC-rich mHtt transgene mRNA to cDNA. The levels of mHtt mRNA were determined using real-time quantitative PCR. Baseline levels of striatal mHtt mRNA were established by analyzing total RNA from striatal tissue contralateral to the rAAV5-shRNA injection. mHtt mRNA levels from control and rAAV5-shRNA injected striatum were normalized to hypoxanthine phosphoribosyl transferase (HPRT) mRNA levels and subjected to one-way ANOVA. Long-term expression of rAAV5-siHUNT-1 or rAAV5-siHUNT-2 in the striatum of the R6/1 mouse resulted in highly significant reductions in the levels of mHtt mRNA (Fig. 3-3C) demonstrating that intrastriatal delivery of rAAV5 anti-mHtt shRNAs in the R6/1mouse can induce efficient knockdown of mHtt mRNA levels. Moreover, this reduction was specific to the expression of rAAV5-siHUNT-1 or –siHUNT-2 since mHtt mRNA levels were unchanged following the expression of rAAV5-siRho-1 (Fig. 3-3C).

To determine the levels of total striatal mHtt protein in the R6/1 mouse, we generated a rabbit polyclonal antibody against a specific peptide in the amino-terminus of human Htt (Hum-1). The Hum-1 antibody recognized a high molecular weight band of greater than 250 kDa that was enriched in nuclear fractions of protein extracts from R6/1 but not wild-type littermate controls (Fig. 3-4A). We measured the relative intensity of the high molecular weight Hum-1 immunoreactive band to compare the levels of mHtt protein in transduced and control R6/1 striatum. We normalized the levels of mHtt

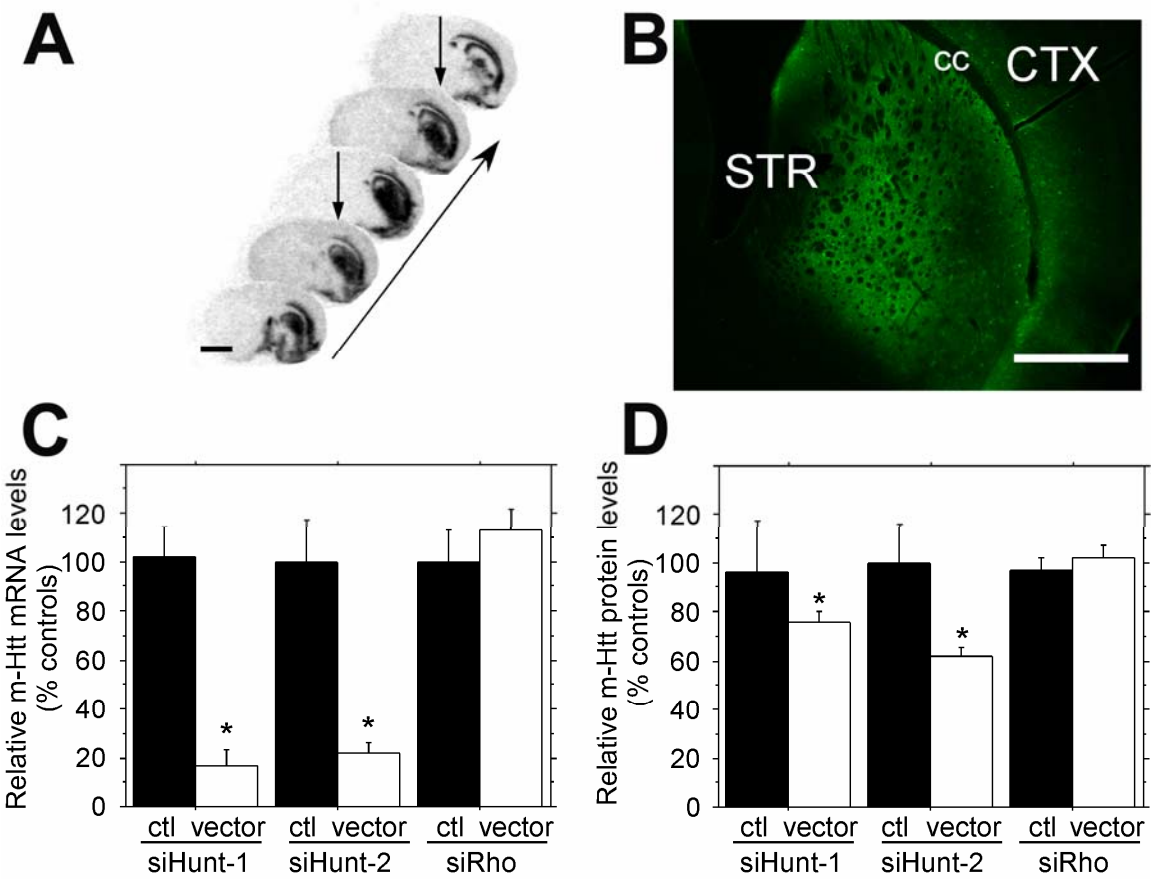

Figure 3-3. Long-term in vivo striatal expression of rAAV5-siHUNT1 and rAAV-siHUNT2 decrease mHtt transgene mRNA expression. A. In situ hybridization with a probe against the virally encoded hrGFP mRNA. Coronal sections were obtained 10 weeks post-surgery. The panel was arranged in a rostral-caudal axis to illustrate the extent of the transduced area as indicated by the arrow. Two separate injections were placed into the same hemisphere (arrows). These sections were obtained from one animal and are representative of all other study animals. Scale bar = 2mm. B. Photomicrograph of native hrGFP protein expression from the striatum of a representative injected animal demonstrates that the vector derived mRNA shown in (A) is transcribed into protein. Str = striatum, cc = corpus callosum, and CTX = cortex. Scale bar = 1mm. C. Real-time quantitative PCR analysis of mHtt mRNA knockdown. Total RNA was extracted from the striata of R6/1 mice. The levels of striatal mHtt mRNA on the uninjected (black bars) striata and injected striata with rAAV5 vectors (white bars). rAAV5-siHUNT-1, rAAV5-siHUNT-2, and rAAV5 siRho were measured, normalized to the levels of HPRT mRNA and reported as percent of control. Expression rAAV5-siHUNT-1 resulted in a significant 75% reduction of mHtt mRNA expression ($F[1,11] = 40.0$ * = $p<0.001$). Striatal rAAV5-siHUNT-2 treatment resulted in significant 78% reduction of striatal mHtt mRNA expression ($F[1.8] = 19.1$, * = $p = 0.002$). In contrast, striatal injection of the control shRNA rAAV5-siRho did not reduce striatal mHtt mRNA levels

Figure 3-3 continued

($F[1,8] = 0.71$, $p > 0.40$). D. Similarly to striatal mRNA analysis in (C), total protein was obtained from the injected and untreated control striata of R6/1 mice. Similar to the mRNA levels, there was a significant rAAV5-sitHUNT-1 mediated 24.5% reduction in the levels of a Hum-1 immunoreactive high molecular weight band (simple main effects, $F[1,18] = 5.2$, * = $p < 0.04$). The rAAV5-siHUNT-2 treated group displayed a significant 38% reduction of striatal mHtt (simple main effects, $F[1,18] = 8.4$, * = $p = 0.01$) while the rAAV-siRho control groups did not have significant reductions of striatal mHtt (simple main effects, $F[1,18] = 0.50$, $p > 0.40$) when compared to R6/1 control striata. Error bars represent +SEM.

protein to a cross-reactive band that was recognized by the Hum-1 antibody and was present at constant levels in protein extracts isolated from R6/1 and wild-type mice. rAAV5-siHUNT-1 and rAAV5-siHUNT-2 also reduced striatal mHtt protein levels but not to the same degree observed with striatal mHtt mRNA levels. Thus, striatal rAAV5-siHUNT-1 expression reduced striatal mHtt protein approximately 25% compared to control striata or rAAV5-siRho treated mice (Fig 3-3D). In addition, rAAV5-siHUNT-2 reduced striatal mHtt protein 38% relative to untreated control striata or rAAV5-siRho injected mice (Fig 3-3D.). Expression of the control shRNA, siRho had no effect on striatal mHtt expression.

There is a clear discrepancy between the magnitude of si-HUNT-1 and si-HUNT-2 mediated mHtt mRNA reduction and the magnitude of reduction of mHtt protein from the same striata. One potential reason for this discrepancy between mRNA and protein is the differential kinetics of turnover of mRNA versus protein. Moreover, our tissue sampling protocol included both transduced and non-transduced cells, which would lead to an underestimate of the effectiveness of mHtt knock-down, although there is no reason why this would differentially affect measured protein levels compared to mRNA levels. In summary, long-term intrastriatal expression of rAAV5-siHUNT-1 and -siHUNT-2 shRNAs significantly reduced striatal mHtt mRNA levels and also resulted in diminished striatal mHtt protein expression.

Reduction in the Size and Amount of NIIs is Observed in R6/1 Mice Treated With rAAV5-siHUNT-1 or rAAV5-siHUNT-2.

One of the pathological markers of disease progression in mouse models of pQ-disease such as HD is the presence of NIIs. Studies have shown that suppressing the expression of the mutant pQ-containing protein in neurons results in the clearance of NIIs

[12; 23]. We examined whether the Hum-1 antibody could detect the presence of NIIs in the R6/1 striatum. We reasoned that using an anti-Htt antibody instead of an anti-ubiquitin antibody would allow us to directly correlate the levels of mHtt with the presence or absence of NIIs. Immunohistochemical analysis of coronal brain sections from untreated R6/1 mice subjected to Hum-1 and anti-ubiquitin immunohistochemistry revealed a similar pattern of immunoreactivity between both antibodies with respect to the size and distribution of NIIs in the R6/1 mouse brain (Fig. 3-4A-D). Histological analysis of sections obtained from R6/1 mice of various ages showed that Hum-1-positive NIIs become visible in the light-microscope at about 8 weeks after birth (data not shown), in agreement with the time that ubiquitin-positive NIIs become visible in the R6/1 mouse [18]. Hum 1- (data not shown) and anti-ubiquitin- [18] immunoreactive NIIs increase in size and staining intensity during the progression of HD suggesting that protein deposition in NIIs is cumulative.

We analyzed Hum-1 immunostained coronal sections from unilaterally injected R6/1 mice and compared the relative area and intensity of NIIs present in four brain regions including the left primary motor cortex, right primary motor cortex, left medial striatum and right medial striatum (Fig. 3-4F). Three of these regions, left primary motor cortex, right primary motor cortex and left medial striatum, corresponded to non-transduced control tissue while the right medial striatum exhibited strong rAAV5-mediated transduction (Fig. 3-3A,B & 3-4F). Comparison of Hum-1 staining in the left and right primary motor cortex revealed no differences in the area or intensity of NIIs in any of the R6/1 mice that were untreated or treated with either rAAV5-siHUNT-1 (Fig. 3-4G & H) or –siHUNT-2 (Fig. 3-4M & N). Areas shown in figure 3-4I,J,K,L,O,P were

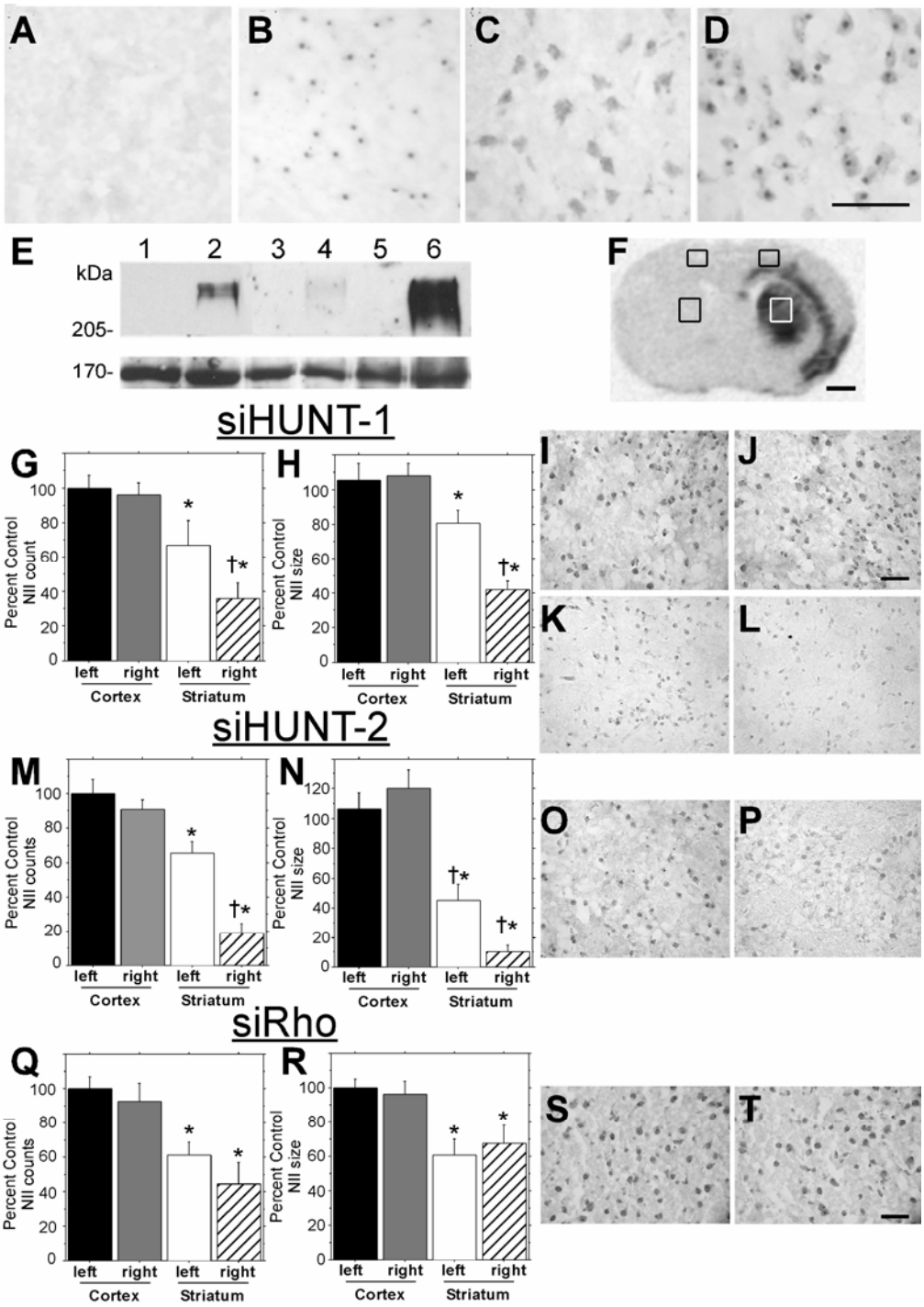

Figure 3-4 Analysis of mHtt protein aggregates after expression of rAAV5-shRNAs**.** A-D. Immunohistochemistry showed that the human Htt amino-terminus-specific antibody Hum-1 antibody, like anti-Ubiquitin antibody, detects NIIs in R6/1 but not wild-type mice. Panels (A) and (B) were striatal sections immuno-stained using an anti-ubiquitin antibody. A. Striatal section from a 15 week-old wild-type mouse. B. Striatal section from a 15 week-old R6/1 mouse. Panels (C) and (D) were immuno-stained using the new Hum-1

Figure 3-4 continued

antibody. C. Striatal Hum-1 immuno-staining from the same 15 week-old wild-type mouse as shown in (A). D. Striatal Hum-1 immuno-staining from the same 15 week-old R6/1 mouse as shown in (B). Similar staining of NIIs was found in both anti-ubiquitin and Hum-1 immuno-stained sections. Cross-reactivity of Hum-1 antibody with cytoplasmic proteins in striatal neurons of both wild-type and R6/1 mice is apparent in (C) and (D). E. Western blot analysis of total (lanes 1 and 2), cytoplasmic (lanes 3 and 4) and nuclear (lanes 5 and 6) protein derived from 15 week-old wild-type (lanes 1, 3 and 5) and R6/1 mice (lanes 2, 4 and 6) using the Hum-1 demonstrated that the antibody detects a high-molecular weight aggregate in R6/1 transgenic mice. The lower panel shows a 170-kDa cross-reacting band that is present in all samples and was used as loading control. F. Coronal section from rAAV5-siHunt-1 injected R6/1 mouse processed for in situ hybridization with a probe against vector specific sequences (as shown in Fig. 3A) to demonstrate the transduction area. The boxes show the areas of Hum-1 staining used for analysis of NII number and size (panels G, H, M, N, Q, R) and the photomicrographs shown in panels (J-L), (O,P), (S,T). G-L. These panels contain the analysis of NII count and size for rAAV-siHUNT-1 injected R6/1 mice. NII analysis from all vector-treated mice took place by examining the transduction area using native hrGFP fluorescence in sections adjacent to the Hum-1 immuno-stained section in order to correctly choose the boxed area depicted in (F) for each section. G. Numbers of NIIs were estimated in cortex and striatum of long-term treated R6/1 mice, compared to identically determined NIIs in control striata and expressed as percent of control frequency. Cerebral cortex in either hemisphere was not transduced by rAAV (F) and served as a region control. Cortical NII numbers were unaffected by striatal injection of rAAV5-siHUNT1 (Fisher's PLSD post hoc test, $p = 0.8$). The frequency of NIIs in cortex was generally greater than in the striatum of the R6/1 mouse ($F[1,20] = 22.0$, $*p < 0.001$). In addition, treatment with rAAV5-siHUNT1 significantly reduced the frequency of striatal NIIs by 31% compared to the control uninjected striatum (Fisher's PLSD post hoc test, † $p = 0.04$). Error bars in (G-H), (M-N) H. Similarly to NII numbers, NIIs are smaller on average in the striatum, regardless of treatment as compared to the NII size in cortex ($F[1,20] = 38.4$,* $p < 0.001$). rAAV5 mediated siHUNT-1 expression reduced the size of the remaining NIIs by 39% compared to the untreated control striatum (post-hoc, † $p = 0.0013$). I. Photomicrograph of left cortical Hum-1 stained coronal section from the area shown in the box in (F) showing frequency of NIIs. J. Photomicrograph of the right cortical region shown in the box in (F). Scale bar = 50 μm and applies to (I,J,L). M-P. These panels contain the data from rAAV-SiHUNT-2 treated R6/1 mice. M. The frequency of NIIs in the R6/1 cortex was, in general, greater than the frequency measured in the striatum ($F[1,20] = 68.4$, * $p < 0.0001$). rAAV5 mediated siHUNT2 expression further significantly reduced the number of striatal NIIs by 47% compared to the left striatum (Fisher's PLSD post hoc test, † $p < 0.0001$). N. Similar to NII frequency, Hum-1 positive cortical NIIs

Figure 3-4 continued

are significantly larger than striatal NIIs ($F[1,20] = 71.1$, * $p < 0.0001$). Striatal siHUNT-2 expression further reduced striatal NII size by 35% compared to the untreated striatum (Fisher's PLSD post hoc test, † $p < 0.03$). O. Photomicrograph from the control left striatal area depicted in (F) from a representative rAAV5-siHUNT-2 treated mouse. P. Photomicrograph from the right rAAV5-siHUNT-2 treated striatum from the same mouse depicted in (O) clearly demonstrating reduced NII frequency and size. It should be noted that untransduced striatal areas had Hum-1 positive NII frequency and size that was indistinguishable from those seen in the opposite control striatum. Q-T. These panels contain the NII analysis from the rAAV5-siRho treated mice that serve as the control shRNA experimental group. Q. Quantitative analysis of NIIs frequency of siRho treated mice. As with the other vector treated groups cortical NIIs were more frequent than Hum-1 positive striatal NIIs ($F[1,12] = 20.5$, * $p = 0.0007$). However, there was no difference between NII number between treated and untreated striata (Fisher's post hoc test, $p > 0.2$). R. Hum-1 positive NIIs are also smaller in striatum as compared to the R6/1 cortex ($F[1,12] = 16.8$, *$p < 0.002$). However, control rAAV5-siRho treated striatal Hum-1 positive NIIs were the same size as those measured in the left, control striatum (Fisher's PLSD post hoc test, $p > 0.5$). S. Representative photomicrograph from the left, untreated cortex of a rAAV-siRho treated R6/1 mouse. T. Representative photomicrograph taken from the transduction area (F) from the right, injected striatum of the same mouse shown in (S). There is no apparent difference in striatal NII frequency and size when compared to the left striatum (S). Scale bar = 50 μm and applies to (O,P, and S). Error bars represent +SEM in (G-H), (M-N), and (Q-R).

taken from the same R6/1 mouse section and are representative of all other rAAV5-siHUNT-1 and -siHUNT-2 treated R6 mice. Hum-1 immunoreactive NIIs in the left (Fig. 3-4K & O) and right (Fig. 3-4O & P) medial striatum were smaller and had less intense staining than those present in the cortical regions of the same R6/1 mouse (Fig. 3-4I vs. 4K). This histological observation was also supported by the quantification of NII count (Fig. 3-4G) and area (Fig. 3-4H, see below).

A comparison of the non-transduced left and transduced right medial striatum regions showed a marked reduction in the intensity of Hum-1 NII staining in the rAAV5-siHUNT-1 (Fig. 3-4L) and rAAV5-siHUNT-2 (Fig. 3-4P) transduced right medial striatum when compared to the left medial striatum (Fig. 3-4 K & P, respectively) of the same animal. This observation was corroborated by the quantification of NIIs (Fig. 3-4G&M) count and area (Fig. 3-4H & N, see below). The reduction in Hum-1 NII staining intensity was more pronounced in sections obtained from rAAV5-siHUNT-2-treated compared to siHUNT-1-treated R6/1 mice. Sections from R6/1 mice treated with either rAAV5-GFP (data not shown) or rAAV5-siRho-1 (Fig. 3-4Q-T) showed no significant difference in the pattern of Hum-1 NII staining between the left and right medial striatum regions (Fig. 3-4S versus 4T). The observation of rAAV5-siHUNT1- and rAAV5-siHUNT-2- mediated reduction of striatal Hum-1 NII staining further corroborates the immuno-blot data indicating reduced striatal mHtt protein in vector-treated striata.

In order to quantify the relative area and amount of NIIs present in shRNA treated striata, we analyzed the same relative four regions shown in figure 3-4F in siHUNT-1 treated (n=11), siHUNT-2 treated (n=6) and siRho-1 (n=4) treated R6/1 mice. The mean

relative area (μm^2) and number of particle (NIIs) counts within a specified area range was calculated for each of the four regions in all of the unilaterally injected R6/1 mice using Image *J* software and reported as percent of the non-transduced corresponding area in the opposite hemisphere. Using different anatomical regions from individual coronal sections as internal controls revealed that medial striatal NIIs displayed reduced frequency as well as reduced two-dimensional area compared to NIIs in motor cortex regardless of vector treatment (Fig. 3-4G & H respectively).

Long-term expression of rAAV5-siHUNT-1 resulted in a significant reduction in both the frequency (31%) and mean area (39%) of NIIs in the transduced right medial striatum when compared to the contralateral non-transduced left medial striatum in the same section (Fig. 3-4G&H respectively). Analysis of the right medial striatum in rAAV5-siHUNT-2 treated sections revealed a mean reduction of 47% in the estimated frequency and of 35% in the mean area of NII particles when compared to the left medial striatum (Fig. 3-4M). There was no significant difference in the number or area of NIIs between the right and left medial striatum of rAAV5-siRho-1 treated R6/1 mice (Fig. 3-4Q & R respectively). Our results show that long-term expression of rAAV5-siHUNT-1 or rAAV5-siHUNT-2 in the R6/1 striatum led to a significant reduction in the area and frequency of striatal NIIs present within the region of viral transduction.

Reduced Levels of Striatal mHtt Affect Levels of Striatal-Specific Transcripts.

Expression of exon 1 of *mHtt* leads to a decrease in the level of a subset of striatal-specific mRNAs of the R6/1 mouse [27] [28] [29-31]. These same transcripts are also reduced in HD patients. At the very least, evaluation of these striatal-specific transcripts can serve as an important metric of disease progression in R6/1 mice. To examine the effects that silencing striatal mHtt expression might have on this molecular phenotype,

we performed *in situ* hybridization analysis of transcripts on coronal sections obtained from unilaterally injected wild-type and R6/1 mice. Sections were hybridized with oligonucleotide probes against preproenkephalin (ppEnk), dopamine- and cAMP-responsive phosphoprotein, 32 kDa (DARPP-32), phosphodiesterase 10A (PDE10A), phosphodiesterase 1B (PDE1B), nerve growth factor inducible-A (NGF*i*-A) and the dopamine type 2 receptor (D2) receptor.

Densitometric analysis of rAAV5-siHUNT-1 injected R6/1 mice showed an increase in the mean levels of striatal ppEnk (24%) and DARPP-32 (16%) mRNA in the transduced striatum (Fig. 3-5A & B) as compared to the contralateral uninjected side. There was no significant side-to-side difference in the levels of PDE10A, PDE-1B, NGF*i*-A or D2 receptor mRNAs in R6/1 mice treated with rAAV5-siHUNT-1 (data not shown).

In contrast, expression of rAAV5-siHUNT-2 in R6/1 mice resulted in a marked decrease in the mean levels of both ppEnk (16%) and DARPP-32 (30%) mRNAs when compared to the uninjected left side (Fig. 3-5C & D). More importantly, this decrease was also evident in unilaterally injected wild-type mice for both ppEnk (75%) & DARPP-32 (56%) mRNAs (Fig. 3-5 panels C & D). This pronounced reduction in mRNA levels was also observed in all other transcripts tested (not shown), except for NGF*i*-A where the long-term expression of siHUNT-2 shRNA led to an increase in transcript levels that exceeded that of wild-type uninjected controls (not shown).

The β-actin-specific hybridization signal remained unchanged in all samples tested. Based on the comparable reduction in transcripts in wild-type and R6/1 mice, we attributed the reduction in the steady-state levels of these striatal-specific transcripts to a

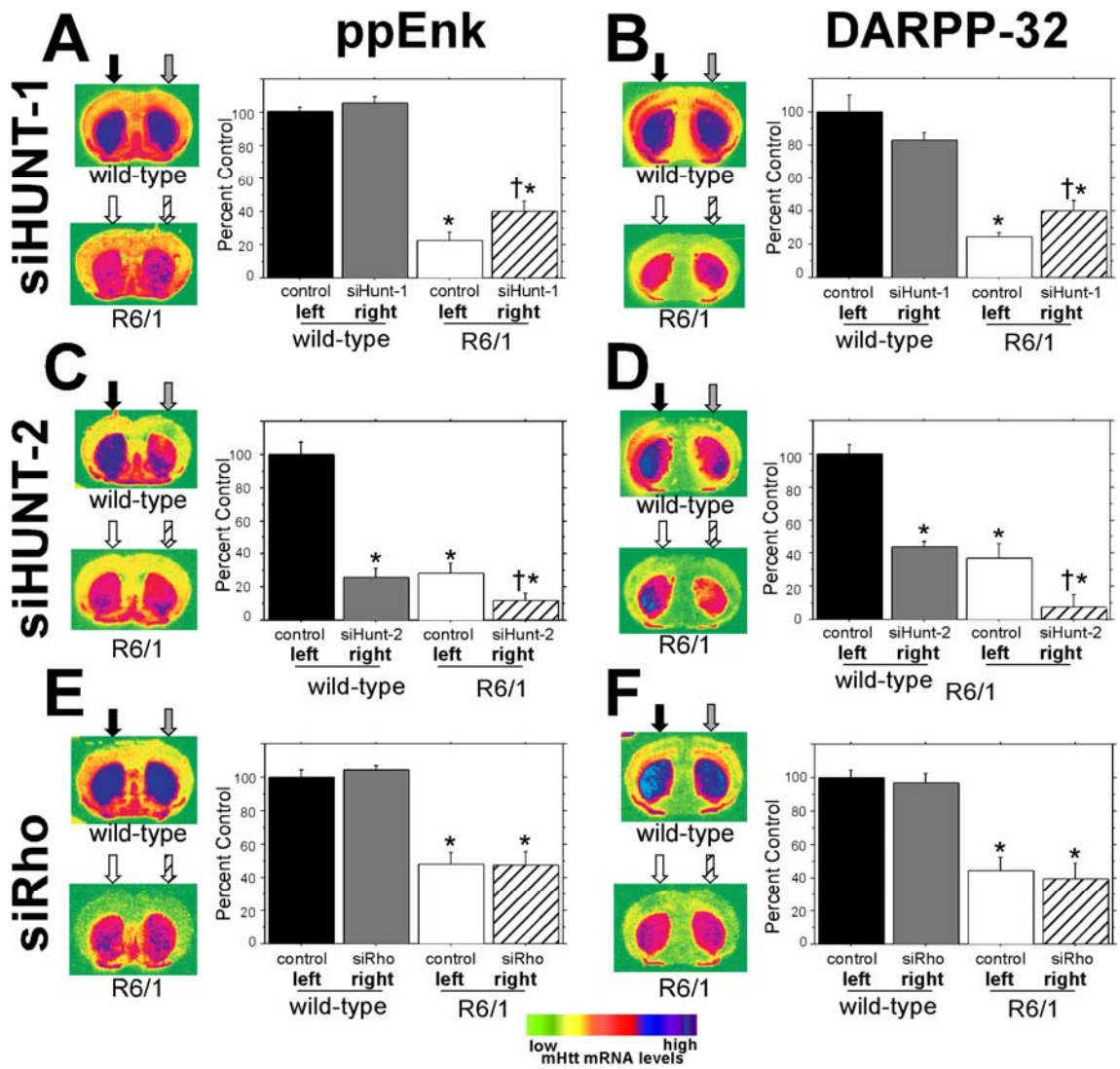

Figure 3-5 In situ hybridization (ISH) analysis of ppEnk and DARPP-32 transcripts. Coronal sections shown to the left of (A), (C), and (E) were hybridized to a ppEnk-specific oligonucleotide probe (Table 1) while sections in panels (B), (D) and (F) were hybridized to a DARPP-32-specific oligonucleotide probe (Table 1). The arrows above the coronal sections show the approximate vector injection site and the fill pattern of the arrows corresponds to the fill pattern of the histograms in each panel to show which treatment was received in each hemisphere. In order to better demonstrate the anatomical pattern of striatal transcripts the coronal sections were false colored. The scale is shown at the bottom of the figure. A. Evaluation of long-term intrastriatal rAAV-siHUNT-1 expression on striatal ppEnk levels in R6/1 mice and wild-type littermate controls. Quantitative analysis of normalized ppENK levels confirm that ppENK levels are reduced in 22 week old R6/1 mice ($F[1,66] = 99.5$, * $p < 0.0001$). rAAV-siHUNT-1 injection into wild-type control striata does not lead to any alteration in striatal ppENK levels as compared to untreated

Figure 3-5 continued

control left striata (Fisher's PLSD post hoc test, $p > 0.7$). In contrast, in R6/1 mice, striatal rAAV5-siHUNT-1 treatment led to a mild 24% increase in striatal ppEnk levels as compared to the ppEnk levels observed in the control striatum (Fisher's PLSD post hoc test, † $p = 0.01$). B. Evaluation of long-term intrastriatal rAAV-siHUNT-1 injection on steady state striatal DARPP-32 mRNA levels. Similar to ppENK mRNA levels, DARPP-32 mRNA was reduced in R6/1 animals as compared to littermate controls ($F[1,66] = 114.1$, * $p < 0.0001$). rAAV5-siHUNT-1 injection did not affect striatal DARPP-32 levels in wild-type controls (Fisher's PLSD post hoc test, * $p > 0.1$). Striatal rAAV5-siHUNT-1 treatment resulted in a significant 16% increase in DARPP-32 mRNA levels (Fisher's PLSD post hoc, † $p < 0.03$) in R6/1 mice as compared to DARPP-32 mRNA levels in the untreated striatum. C. Analysis of the effect of intrastriatal injection of rAAV-siHUNT-2 on striatal ppEnk transcript levels. In stark contrast to the pattern seen with rAAV5-siHUNT-1 injection (A), rAAV5-siHUNT-2 long-term expression led to a 75% reduction of striatal ppENK levels in the injected striatum of wild-type littermate controls (Fisher's PLSD post hoc test, *$p < 0.0001$). Likewise, rAAV5-siHUNT-2 treatment also resulted in a further 16% reduction in striatal ppENK levels in R6/1 mice (Fisher's PLSD post hoc test, † $p < 0.05$). D. Analysis of the effect of intrastriatal injection of rAAV-siHUNT-2 on striatal DARPP-32 mRNA levels. Similar to the pattern seen in response to rAAV5-siHUNT-2 expression striatal ppEnk levels (C), rAAV5-siHUNT-2 long-term expression led to a 44% reduction of striatal DARPP-32 mRNA levels in the injected striatum of wild-type littermate controls (Fisher's PLSD post hoc test, *$p = 0.0005$). In addition, rAAV5-siHUNT-2 treatment resulted in a further 70% reduction in striatal DARPP-32 mRNA levels in R6/1 mice (Fisher's PLSD post hoc test, † $p < 0.01$). This further reduction in the treated striatum of the R6/1 mice is particularly apparently in the right side of the coronal section shown to the right of the histogram in this panel. E. Evaluation of the effect of the long-term expression of the control shRNA, siRho in the striatum of wild-type littermate controls and R6/1 mice on striatal ppEnk levels. rAAV5-siRho injections had no effect on striatal ppEnk transcript levels in either wild-type controls (Fisher's PLSD post hoc test, $p > 0.9$) or R6/1 mice (Fisher's PLSD post hoc test, $p > 0.6$). F. Evaluation of the effect of the long-term expression of the control shRNA, siRho in the striatum of wild-type littermate controls and R6/1 mice on striatal DARPP-32 mRNA levels. rAAV5-siRho injections had no effect on striatal DARPP-32 mRNA levels in either wild-type controls (Fisher's PLSD post hoc test, $p > 0.7$) or R6/1 mice (Fisher's PLSD post hoc test, $p > 0.6$). Error bars are + SEM.

siHUNT-2 shRNA-mediated "off-targeting" effect. Further documentation of this important off-targeting finding is the subject of a separate study (Rodriguez et al., in preparation).

Analysis of R6/1 mice injected unilaterally with the control rAAV5-siRho-1 shRNA revealed no significant differences in the levels of ppEnk, DARPP-32, PDE10A, PDE-1B, NGF*i*-A or D2 receptor mRNA between the left uninjected and right injected striatum (Fig. 3-5E & F). Additionally, there was no side-to-side difference in the steady-state levels of any of the transcripts analyzed in the striatum of wild-type mice injected unilaterally with rAAV5-siHUNT-1 (Fig 3-5A&B). We conclude that rAAV5-siHUNT-1 mediated reduction of mHtt levels in the striatum of R6/1 mice resulted in a small but significant increase in the steady-state levels of striatal ppEnk and DARPP-32 mRNAs relative to the levels observed in the untreated contralateral striatum.

Long-Term Bilateral Striatal Expression of rAAV5-siHUNT-1 in the R6/1 Mouse is Associated With a Delay in the Clasping Phenotype.

R6/1 mice display a progressive neurological phenotype that includes clasping of the hind limbs, and dyskinesias (10). Additionally, R6/1 fail to gain weight at a normal rate and show a progressive decrease in retention times in the rotarod when compared to age-matched wild-type littermate mice. In order to examine whether lowering the striatal levels of mHtt would prevent the progression of these phenotypes, 6-8 week old R6/1 and wild-type mice were injected bilaterally at two different striatal sites (4 injections total) with rAAV5-siHUNT-1 or rAAV5-GFP control. We initially assessed the progression of the HD-like phenotype in the R6/1 mice by recording weights weekly beginning at 1 week post-surgery.

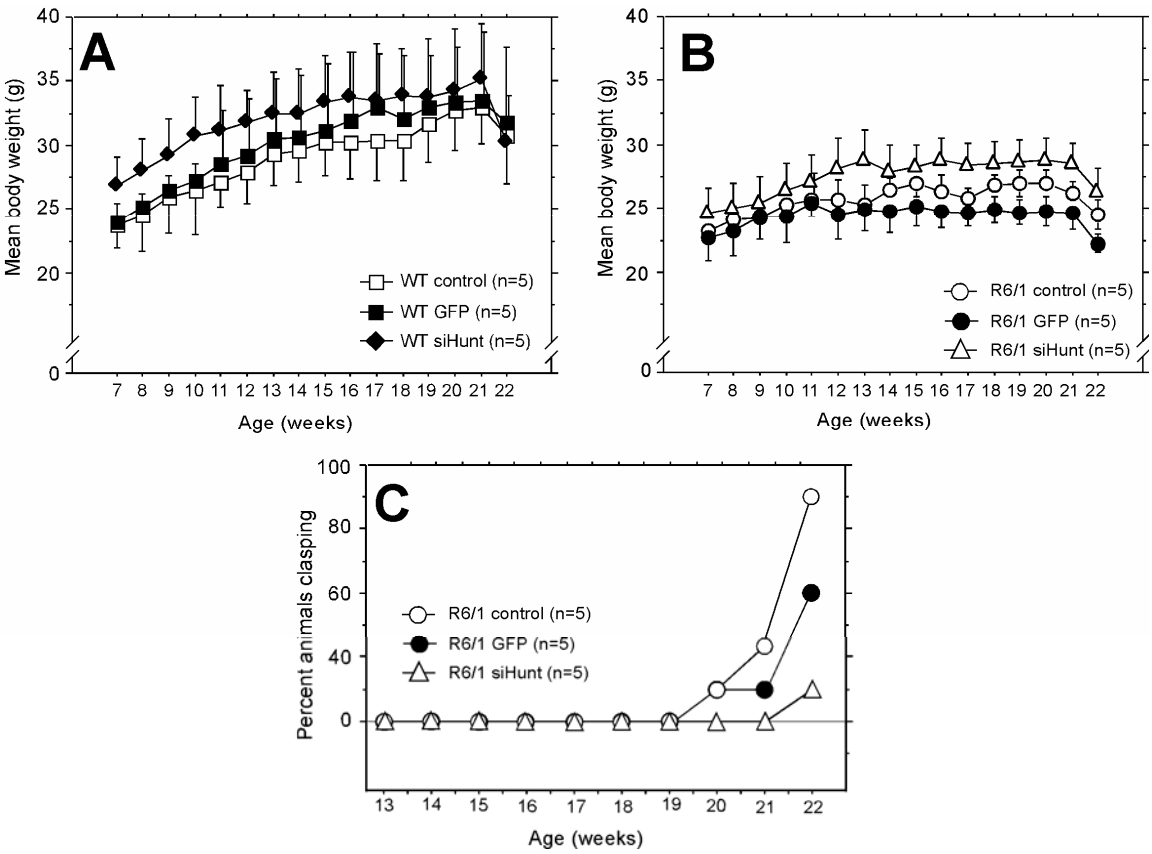

Figure 3-6 Bilateral long-term striatal expression of rAAV5-siHUNT-1 delays the clasping phenotype of R6/1 mice. A. Animal weight was recorded weekly starting at 1 week post-surgery (Fig. 2B). A. The mean (±SEM) weight for wild-type littermate controls is shown. The symbol key is given in the lower right corner of the graph. There was no effect of rAAV-siHUNT-1 treatment on weight regardless of genetic background or vector treatment including rAAV5-GFP (rAAVrepeated measures ANOVA, $F[2,22] = 0.63$, $p > 0.5$). B. The mean (±SEM) weight for R6/1 mice is shown. In general, R6/1 mice weighed less than aged-matched littermate controls ($n = 5$) over the period of the experiment ($F[1,22] = 4.7$, $p = 0.04$ A vs. B).C. Tail-suspension tests were performed weekly beginning at 6 weeks post-surgery (corresponding to 13 weeks of age) on age-matched control R6/1 mice (n=5) and R6/1 mice injected bilaterally with rAAV5-siHUNT-1 (n=5) or rAAV5-GFP (n=5). Data are presented as percent of animals scoring positive for the test as a function of time. Open circles denote age-matched control R6/1. Closed circles denote R6/1 rAAV5-GFP. Open triangles denote R6/1 rAAV5-siHUNT-1.

As previously reported, we observed that R6/1 mice did not increase total body weight at the same rate over time compared to age-matched wild-type littermate mice

(Fig. 3-6A versus B). Examination of the mean weekly weights of uninjected wild-type mice and wild-type mice injected with rAAV5-GFP or rAAV5-siHUNT-1 revealed that long-term expression of neither viral vector led to a significant change in the rate of weight gain over the experimental period (Fig.3-6A). Similarly, long-term expression of neither rAAV5-GFP nor rAAV5-siHUNT-1 in R6/1 mice resulted in a significant change in rate of weight gain when compared to untreated R6/1 (Fig. 3-6B).

We also analyzed the progression of the clasping phenotype in uninjected, rAAV5-GFP or rAAV5-siHUNT-1 injected R6/1 mice by performing a weekly tail-suspension test beginning at 13 weeks of age. Uninjected and rAAV5-GFP injected R6/1 mice began to display clasping of the hind limbs at 20 weeks of age. In contrast, R6/1 mice expressing rAAV5-siHUNT-1 did not show evidence of clasping until 22 weeks of age, when only 20% overtly displayed the phenotype in comparison with up to 80% of uninjected and rAAV5-GFP injected R6/1 mice, which overtly displayed the hind limb clasping phenotype at this same time point.

Finally, we examined the locomotor activity, as determined by total distance traveled, and rotarod retention times of both wild-type and R6/1 mice 16 weeks post-surgery (22 weeks of age). Although there were significant differences between wild-type and R6/1 mice in both tasks, we observed no significant differences among uninjected, rAAV5-GFP and rAAV5-siHUNT-1 injected R6/1 mice in either total distance traveled over time or rotarod retention times (data not shown).

We conclude that 6-8 week old mice expressing rAAV5-siHUNT-1 bilaterally in the striatum for up to 14 weeks did not display any overt toxicity associated with our gene transfer approach. Furthermore, long-term expression of siHUNT-1 anti-mHtt

shRNA resulted in a mild behavioral improvement of the R6/1 phenotype with respect to clasping behavior but did not affect body weight abnormalities or muscle-dependent activities such as rotorod retention and locomotion.

Discussion

The expression of one expanded *HD* allele initiates a cascade of events that leads to the neuronal dysfunction and pathology observed in HD (81). It has been hypothesized that ablating the expression of mHtt might protect against or even reverse the effects associated with poly-Q expanded Htt protein. In this study, we assessed the molecular and behavioral effects of long-term intrastriatal rAAV5-mediated expression of shRNAs designed to suppress the expression of the human *mHtt* transgene that is present in R6/1 mice. Our results demonstrate that post-transcriptional gene silencing of striatal mHtt in adult R6/1 mice by one of two shRNAs tested, siHUNT-1, has a mild positive effect on the rapid cellular and behavioral pathological changes that occur in this model. At the cellular level, improvement occurred in only 2 striatal specific transcripts and this amelioration was only found in the striatal subregion of rAAV5-mediated transduction. These data therefore suggest that greater transduction efficiency could improve the functional effects obtained here.

Intrastriatal injections of rAAV5 vectors resulted in widespread transduction of the mouse striatum especially as compared to previously reported levels of transduction in mice (35; 36). Long-term expression of rAAV5-siHUNT-1 in the R6/1 mouse striatum resulted in mRNA levels that were reduced by 75% when compared to controls while reduction in protein levels ranged from 25-38%. Aggregated, but not soluble, mHtt was detected using our western blot protocol, which may have contributed to the discrepancy between the magnitude of reduction of mRNA and mHtt protein. In fact, even though we

tested several published antibodies and a variety of extraction protocols, we were unable to detect measurable levels of soluble mHtt N-terminal fragments in total striatal protein samples from untreated adult R6/1 mice.

In agreement with the data obtained from Hum-1 immuno-blots indicating reduced striatal mHtt in transduced regions, Hum-1 immunohistochemical analysis of sections from rAAV5-siHUNT-1 treated R6/1 mice revealed a marked decrease in the size and number of NIIs within the area of viral transduction. Thus, since aggregation of soluble mHtt fragments leads to the formation of inclusions *in vivo*, our data suggest that expression of rAAV5-siHUNT-1 significantly diminished the available cellular pool of soluble mHtt N-terminal fragments in the striatum of the R6/1 mouse.

The functional significance of NIIs in HD mouse models is currently controversial. NIIs have been hypothesized to be a protective mechanism in cells by functioning to sequester detrimental toxic forms of Htt from damaging the cell (37). On the other hand, NIIs may also be a pathological feature causing transcriptional dysregulation via binding of vital transcription factors and sequestering these factors from regulatory sequences. Along these lines, mHtt has been shown to affect the cellular localization and function of several regulators of transcription known to be critical for proper neuronal function, which results in the specific down-regulation of a subset of striatal mRNAs (38).

Expression of rAAV5-siHUNT-1 in the striatum of the R6/1 mouse resulted in a significant increase in the steady-state mRNA levels of both ppEnk and DARPP-32 mRNAs as demonstrated by *in situ* hybridization analysis. No significant changes were observed in either the dopamine type-2 receptor or NGF*i*-A mRNA levels. Additionally, expression of rAAV5-GFP or the inactive control shRNA, rAAV5-siRho-1, did not result

in any detectable changes in the levels of any of the transcripts analyzed. The promoter for ppEnk is regulated by the cAMP-responsive element (CRE-) transcriptional pathway (39). The CRE-transcriptional pathway is extensively involved in the regulation of genes needed for neuronal function and survival, and expression of mHtt has been shown to interfere with this pathway (40-42). CRE-mediated transcription is modulated by $TAF_{II}130$, and the pQ domain of soluble mHtt N-terminal fragments can sequester $TAF_{II}130$, into aggregates. This aberrant protein-protein interaction is thought to negatively affect CRE-regulated transcription by affecting the proper localization and function of $TAF_{II}130$ (41). Therefore, reduced levels of striatal mHtt might have a direct effect on the activity of CRE-mediated transcription. In this study, while the frequency and size of NIIs were reduced and disease-affected striatal transcripts were improved by administration of siHUNT-1, the relationship between NIIs and disease progression and the exact role of mHtt in transcriptional dysregulation remains poorly understood.

We have observed that the levels for both ppEnk and DARPP-32 mRNA begin to decrease at ~ 4-5 weeks of age and reach a minimum steady-state level around 12 weeks of age (Denovan-Wright, unpublished data). In this study, we initiated shRNA treatment to reduce striatal mHtt expression in R6/1 mice that were between 6 and 8 weeks of age. Since we did not fully restore ppENK and DARPP-32 mRNAs to wild-type levels, our data suggests that lowering the levels of striatal mHtt affected the rate of loss in steady-state mRNA levels. Alternatively, R6/1 striatal neurons expressing low levels of mHtt protein may have maintained an increased level of transcriptional activity when compared to striatal neurons expressing normal levels of mHtt.

Finally, we investigated whether long-term expression of rAAV5-siHUNT-1 would affect the behavioral phenotype displayed in the R6/1 mouse. In this study, we evaluated a battery of physiological and behavioral tests including effect on weight loss, clasping phenotype, locomotor activity, and performance on the rotarod apparatus. There was no difference in weight among the groups of R6/1 mice bilaterally treated with rAAV5-siHUNT-1, rAAV5-GFP R6/1 and uninjected age-matched R6/1 controls. Additionally, locomotor activity remained unchanged in rAAV5-siHUNT-1 treated R6/1 when compared to controls. Analysis of retention times in the rotarod apparatus demonstrated a clear difference between genotype; however, we observed no differences between all of the three different R6/1 groups. In contrast, there was a delayed onset of the clasping-phenotype on R6/1 mice that were bilaterally injected with rAAV5-siHUNT-1 when compared to uninjected or rAAV5-GFP injected R6/1 mice. This mild behavioral improvement may suggest that suppression of mHtt expression in other regions of the brain, i.e. cortex, may be required in order to achieve a more explicit positive effect on behavior. Also, some of the behavioral phenotypes observed in the R6/1 mouse may be affected by dysfunction of other systems outside the CNS. In fact, problems with metabolism and muscle wasting have been observed in the R6 lines (43). These systemic abnormalities would not be expected to improve after suppression of striatal mHtt expression.

In addition to the observation that siHUNT-1 reduced mHtt levels and had a positive effect on the cellular and behavioral phenotype of R6/1 mice, we observed that another active anti-mHtt shRNA, siHUNT-2, reduced levels of striatal-specific transcripts in wild-type and R6/1 mice indicating that this molecule had deleterious effects that were

independent of mHtt knock-down. As shown by these results, extreme caution should be taken when interpreting data from shRNAs *in vivo* and that detailed analysis of cellular gene expression can detect off-targeting effects associated with the intracellular expression of shRNAs.

In conclusion, long-term rAAV5-mediated striatal expression of an anti-mutant Htt shRNAs was well tolerated in both wild-type and R6/1 transgenic mice and leads to changes that are consistent with reduced expression levels of mHtt protein. Moreover, improved striatal transduction, use of a slower progressing HD mouse model, transduction in additional critical brain regions such as cerebral cortex, intervention earlier in the time-course of pathology, or a combination of these factors may lead to better shRNA-mediated striatal mHtt knock-down effects. Nevertheless, we have demonstrated that reduced levels of striatal mHtt can be achieved through the use of RNAi and that this treatment results in a mildly improved cellular and behavioral phenotype in the R6/1 line of HD. Since polymorphisms associated with the *mHtt* allele have been described (44-46), these results suggest that mutant allele specific gene silencing may be a clinically viable approach once remaining efficiency and safety issues are resolved (19,34).

CHAPTER 4
CONCLUSIONS

HUNTINGTON'S DISEASE (HD) is a severe and fatal autosomal dominant neurological disorder characterized by a late onset of motor and cognitive deficits including involuntary movements and phsychiatric manifestations. Inheritance of an abnormally expanded CAG-triplet repeat region is the genetic factor responsible for HD. This expansion is translated into a poly-glutamine (pQ) domain in the N-terminus of a protein termed huntingtin. Expression of this protein initiates the pathological molecular cascade of events that leads, without remission, to death of the affected individual within 20 years after the presentation of symtpoms. At the time that these studies were completed, there existed no clinical treatment to successfully slow down disease progression.

Progression of HD is dependent on sustained mutant huntingtin expression. Therefore, we hypothesized that reduced levels of striatal m-Htt would slow down the rate of disease progression in a transgenic mouse model of HD. In order to test this hypothesis, we tested the ability of anti-mutant huntingtin hammerhead ribozymes and anti-mutant huntingtin shRNAs to mediate post-transcriptional silencing of m-Htt expression in vivo. We specifically characterized the effect that the long-term expression of anti-mutant huntingtin hammerhead ribozymes and anti-mutant huntingtin shRNAs had on neuronal intranuclear inclusion (NIIs) bodies and the progressive transcriptional dysregulation phenotype displayed in the R6/1 transgenic HD mouse line.

We have demonstrated that long-term expression of rAAV5-siHUNT-1 short-hairpin RNA against m-Htt RNA led to significant silencing of m-Htt expression in the striatum of the R6/1 mouse (Chapter 4). Furthermore, RNAi-mediated silencing of m-Htt expression led to a significant decrease in the size and numbers of neuronal intranuclear inclusions, a marker of disease progression in the R6/1 mouse. In addition, in situ hybridization analysis demonstrated that reduced striatal levels of m-Htt led to an increase in the steady-state mRNA levels of both ppEnk and DARPP-32 but not of the dopamine type-2 and NGFi-A transcripts. Finally, we showed that long-term bilateral striatal expression of rAAV5-siHUNT-1 led to a delayed in the onset of the clasping phenotype displayed by R6/1 mice.

We are the first to demonstrate that long-term striatal expression of anti-mutant Htt shRNAs result in reduced levels of m-Htt protein *in vivo* in the R6/1 model of HD. We also showed that this reduction resulted in a decrease in the size and amount of NIIs, concomitant with an increase in the mRNA steady-state levels of ppEnk and DARPP-32 and a delayed in the clasping phenotype in the R6/1 mouse.

Unresolved Issues

The function of wild-type Htt remains unknown. Although there is data supporting a role for Htt in neuronal survival, these studies have focused on the ablation of Htt expression prior to neuronal survival. Our experimental approach tested the hypothesis that the specific knockdown of striatal m-Htt protein would lead to a slower progression of the HD phenotype in the R6/1 mouse. Allele-specific silencing of m-Htt, while plausible in a transgenic mouse line, will be extremely difficult to achieve within the context of the human genome. In HD, the inheritance and expression of one CAG-expanded allele leads to disease. shRNAs directed against the CAG domain in huntingtin,

although efficient in silencing m-Htt expression, can not discriminate between the mutant and wild-type alleles. Silencing of wild-type Htt in adult neurons could lead to neurodegeneration. To circumvent these problems, synthetic siRNAs directed against polymorphisms linked with the mutant allele have successfully reduced the levels of the mutant allele while minimally affecting the levels of wild-type protein. However, this has yet to be proven in vivo where the effects of off-targeting remain relatively unknown.

Long-term in vivo expression of both HD6 and HD7 hammerhead ribozymes as well as the siHUNT-2 shRNA resulted in the remarkable loss of ppEnk, DARPP-32 and dopamine type-2 receptor mRNA steady-state levels in both R6/1 and wild-type mice. This reduction if striatal-specific mRNAs was not due to a global reduction in transcriptional activity since NGFi-A mRNA was induced above wild-type levels (Chapter 3). These three molecules targeted a 22-nucleotide region of the human Htt mRNA. HD6 was designed to target nucleotides at positions 29-41 from the ATG start site of the human Htt mRNA (accession # L34020). HD7 targeted nucleotides at positions 38-49 from the ATG start site while the shRNA siHUNT-2 targeted nucleotides at positions 24-45 from ATG start site. BLAST searches have revealed no similarity to known mouse mRNA sequences, however, there are up to six expressed-sequence tags (ESTs) from adult mouse neurospheres that match the criteria required for the HD6, HD7 or siHUNT-2-mediated cleavage of the molecule. Because the phenotype associated with the expression of HD6 , HD7 and siHUNT-2 was reminiscent to an HD-like phenotype, further studies into the gene or genes that are being directly affected by these molecules are warranted. One initial approach would be to isolate the genes from neurospheres using the EST sequences as probes. One could then design ribozymes or shRNAs against

different and unique sequences within the gene or genes in order to determine their contribution to the HD-like phenotype that we observed.

Future Studies

We report a mild-behavioral improvement in the R6/1 mouse induced by the long-term expression of rAAV5-siHUNT-1. The R6/1 more accurately replicates Juvenile HD were the progression of disease is much faster and severe. Therefore, the fact that we only attained mild cellular and behavioral improvements in the R6/1 mice does not diminish the potential therapeutic value of shRNAs in HD, especially on the more slow-progressing, adult-onset type. In fact, others have evaluated the therapeutic potential of a variety of molecules and environmental enrichment in the R6/1 mouse. These studies have resulted in varying degrees of success that paralleled the findings in our study. For example, the administration of fatty acids led to motor improvements but no recovery in the levels of D1 or D2 mRNA levels. Also, environmentally enriched R6/1 mice have increased rotarod rentention times when compared to controls, however, levels of D1 or D2 mRNAs remained unchanged. Finally, cortical transplantation of wild-type donor cortical tissue results in a delayed in the rear paw clasping phenotype. Thus, the mild improvements attained in our study could translate into more profound effects in slower progressing models of HD.

At the time of this study, RNA*i* was an exciting, albeit, relatively new and unknown mechanism. New understandings of the pathway and the biochemical properties of the RISC complex have paved the way for the development of more specific and more efficient short-hairpin RNAs. This in turn has greatly enhanced the application of shRNAs in animal models of neurological disease. However, issues concerning intracellular expression and delivery into target sites are just now beginning to be

addressed. Developing drug-regulatable expression cassettes and enhancing the capacity of viral vectors to spread into and be contained within target structures will expand the application of RNA*i* from therapy into the study of gene function *in vivo*.

The search for a cure to Huntington's disease not only entails the development of therapies but also the design and application of molecular techniques that will allow the HD research community to unravel the molecular cascade of events that lead to death. This study demonstrated the therapeutic potential of RNA*i*-meditated knockdown of striatal m-Htt. In addition, we also demonstrate that shRNAs can be used to understand gene function in a temporal and spatial manner.

LIST OF REFERENCES

1. **Afione, S. A., J. Wang, S. Walsh, W. B. Guggino, and T. R. Flotte.** 1999. Delayed expression of adeno-associated virus vector DNA. Intervirology **42:**213-20.

2. **Arrasate, M., S. Mitra, E. S. Schweitzer, M. R. Segal, and S. Finkbeiner.** 2004. Inclusion body formation reduces levels of mutant huntingtin and the risk of neuronal death. Nature **431:**805-10.

3. **Aylward, E. H., A. M. Codori, A. Rosenblatt, M. Sherr, J. Brandt, O. C. Stine, P. E. Barta, G. D. Pearlson, and C. A. Ross.** 2000. Rate of caudate atrophy in presymptomatic and symptomatic stages of Huntington's disease. Mov. Disord. **15:**552-60.

4. **Bankiewicz, K. S., S. E. Leff, D. Nagy, S. Jungles, J. Rokovich, K. Spratt, L. Cohen, M. Libonati, R. O. Snyder, and R. J. Mandel.** 1997. Practical aspects of the development of ex vivo and in vivo gene therapy for Parkinson's disease. Exp. Neurol. **144:**147-56.

5. **Bartolome, J., I. Castillo, and V. Carreno.** 2004. Ribozymes as antiviral agents. Minerva. Med. **95:**11-24.

6. **Bates, G.** 2003. Huntingtin aggregation and toxicity in Huntington's disease. Lancet **361:**1642-4.

7. **Bates, G. P., L. Mangiarini, and S. W. Davies.** 1998. Transgenic mice in the study of polyglutamine repeat expansion diseases. Brain Pathol. **8:**699-714.

8. **Bjorklund, A., D. Kirik, C. Rosenblad, B. Georgievska, C. Lundberg, and R. J. Mandel.** 2000. Towards a neuroprotective gene therapy for Parkinson's disease: use of adenovirus, AAV and lentivirus vectors for gene transfer of GDNF to the nigrostriatal system in the rat Parkinson model. Brain Res. **886:**82-98.

9. **Boado, R. J., A. Kazantsev, B. L. Apostol, L. M. Thompson, and W. M. Pardridge.** 2000. Antisense-mediated down-regulation of the human huntingtin gene. J. Pharmacol. Exp. Ther. **295:**239-43.

10. **Bolivar, V. J., K. Manley, and A. Messer.** 2004. Early exploratory behavior abnormalities in R6/1 Huntington's disease transgenic mice. Brain Res. **1005:**29-35.

11. **Bonilla, E.** 2000. [Huntington disease. A review]. Invest. Clin. **41:**117-41.

12. **Boutell, J. M., P. Thomas, J. W. Neal, V. J. Weston, J. Duce, P. S. Harper, and A. L. Jones.** 1999. Aberrant interactions of transcriptional repressor proteins with the Huntington's disease gene product, huntingtin. Hum. Mol. Genet. **8:**1647-55.

13. **Burger, C., O. S. Gorbatyuk, M. J. Velardo, C. S. Peden, P. Williams, S. Zolotukhin, P. J. Reier, R. J. Mandel, and N. Muzyczka.** 2004. Recombinant AAV viral vectors pseudotyped with viral capsids from serotypes 1, 2, and 5 display differential efficiency and cell tropism after delivery to different regions of the central nervous system. Mol. Ther. **10:**302-17.

14. **Cha, J. H.** 2000. Transcriptional dysregulation in Huntington's disease. Trends Neurosci. **23:**387-92.

15. **Daly, T. M.** 2004. Overview of adeno-associated viral vectors. Methods Mol. Biol. **246:**157-65.

16. **Davidson, B. L., and H. L. Paulson.** 2004. Molecular medicine for the brain: silencing of disease genes with RNA interference. Lancet Neurol. **3:**145-9.

17. **Deocaris, C. C., S. C. Kaul, K. Taira, and R. Wadhwa.** 2004. Emerging technologies: trendy RNA tools for aging research. J. Gerontol. A. Biol. Sci. Med. Sci. **59:**771-83.

18. **Dorsett, Y., and T. Tuschl.** 2004. siRNAs: applications in functional genomics and potential as therapeutics. Nat. Rev. Drug. Discov. **3:**318-29.

19. **Dragatsis, I., M. S. Levine, and S. Zeitlin.** 2000. Inactivation of Hdh in the brain and testis results in progressive neurodegeneration and sterility in mice. Nat. Genet. **26:**300-6.

20. **Ferro, P., R. dell'Eva, and U. Pfeffer.** 2001. Are there CAG repeat expansion-related disorders outside the central nervous system? Brain Res. Bull. **56:**259-64.

21. **Flotte, T. R., S. A. Afione, and P. L. Zeitlin.** 1994. Adeno-associated virus vector gene expression occurs in nondividing cells in the absence of vector DNA integration. Am. J. Respir. Cell Mol. Biol. **11:**517-21.

22. **Funato, T.** 2005. Utility of antioncogene ribozymes and antisense oligonucleotides in reversing drug resistance. Methods Mol. Med. **106:**215-33.

23. **Galvao, R., L. Mendes-Soares, J. Camara, I. Jaco, and M. Carmo-Fonseca.** 2001. Triplet repeats, RNA secondary structure and toxic gain-of-function models for pathogenesis. Brain Res. Bull. **56:**191-201.

24. **Gardian, G., and L. Vecsei.** 2004. Huntington's disease: pathomechanism and therapeutic perspectives. J. Neural. Transm. **111:**1485-94.

25. **Gauthier, L. R., B. C. Charrin, M. Borrell-Pages, J. P. Dompierre, H. Rangone, F. P. Cordelieres, J. De Mey, M. E. MacDonald, V. Lessmann, S. Humbert, and F. Saudou.** 2004. Huntingtin controls neurotrophic support and survival of neurons by enhancing BDNF vesicular transport along microtubules. Cell **118:**127-38.

26. **Grimm, D.** 2002. Production methods for gene transfer vectors based on adeno-associated virus serotypes. Methods **28:**146-57.

27. **Grimm, D., and J. A. Kleinschmidt.** 1999. Progress in adeno-associated virus type 2 vector production: promises and prospects for clinical use. Hum. Gene Ther. **10:**2445-50.

28. **Grunewald, T., and M. F. Beal.** 1999. Bioenergetics in Huntington's disease. Ann. N. Y. Acad. Sci. **893:**203-13.

29. **Gusella, J. F., M. E. MacDonald, C. M. Ambrose, and M. P. Duyao.** 1993. Molecular genetics of Huntington's disease. Arch. Neurol. **50:**1157-63.

30. **Hackam, A. S., J. G. Hodgson, R. Singaraja, T. Zhang, L. Gan, C. A. Gutekunst, S. M. Hersch, and M. R. Hayden.** 1999. Evidence for both the nucleus and cytoplasm as subcellular sites of pathogenesis in Huntington's disease in cell culture and in transgenic mice expressing mutant huntingtin. Philos. Trans. R. Soc. Lond. B. Biol. Sci. **354:**1047-55.

31. **Hansson, O., J. Nylandsted, R. F. Castilho, M. Leist, M. Jaattela, and P. Brundin.** 2003. Overexpression of heat shock protein 70 in R6/2 Huntington's disease mice has only modest effects on disease progression. Brain Res. **970:**47-57.

32. **Harjes, P., and E. E. Wanker.** 2003. The hunt for huntingtin function: interaction partners tell many different stories. Trends Biochem. Sci. **28:**425-33.

33. **Hasholt, L., K. Abell, A. Norremolle, C. Nellemann, K. Fenger, and S. A. Sorensen.** 2003. Antisense downregulation of mutant huntingtin in a cell model. J. Gene Med. **5:**528-38.

34. **Hauswirth, W. W., and A. S. Lewin.** 2000. Ribozyme uses in retinal gene therapy. Prog. Retin. Eye Res. **19:**689-710.

35. **Hauswirth, W. W., Q. Li, B. Raisler, A. M. Timmers, K. I. Berns, J. G. Flannery, M. M. LaVail, and A. S. Lewin.** 2004. Range of retinal diseases potentially treatable by AAV-vectored gene therapy. Novartis Found. Symp. **255:**179-88; discussion 188-94.

36. **Hebb, A. L., H. A. Robertson, and E. M. Denovan-Wright.** 2004. Striatal phosphodiesterase mRNA and protein levels are reduced in Huntington's disease transgenic mice prior to the onset of motor symptoms. Neuroscience **123:**967-81.

37. **Hermonat, P. L., and N. Muzyczka.** 1984. Use of adeno-associated virus as a mammalian DNA cloning vector: transduction of neomycin resistance into mammalian tissue culture cells. Proc. Natl. Acad. Sci. U S A **81:**6466-70.

38. **Ho, L. W., J. Carmichael, J. Swartz, A. Wyttenbach, J. Rankin, and D. C. Rubinsztein.** 2001. The molecular biology of Huntington's disease. Psychol. Med. **31:**3-14.

39. **Humbert, S., and F. Saudou.** 2004. [Stimulation of BDNF transport by huntingtin]. Med. Sci. (Paris) **20:**952-4.

40. **Huntington, G.** 2003. On chorea. George Huntington, M.D. J. Neuropsychiatry Clin. Neurosci. **15:**109-12.

41. **Jiang, H., F. C. Nucifora, Jr., C. A. Ross, and D. B. DeFranco.** 2003. Cell death triggered by polyglutamine-expanded huntingtin in a neuronal cell line is associated with degradation of CREB-binding protein. Hum. Mol. Genet. **12:**1-12.

42. **Kamiya, H., H. Akita, and H. Harashima.** 2003. Pharmacokinetic and pharmacodynamic considerations in gene therapy. Drug Discov. Today **8:**990-6.

43. **Kearns, W. G., S. A. Afione, S. B. Fulmer, M. C. Pang, D. Erikson, M. Egan, M. J. Landrum, T. R. Flotte, and G. R. Cutting.** 1996. Recombinant adeno-associated virus (AAV-CFTR) vectors do not integrate in a site-specific fashion in an immortalized epithelial cell line. Gene Ther. **3:**748-55.

44. **Keene, C. D., C. M. Rodrigues, T. Eich, M. S. Chhabra, C. J. Steer, and W. C. Low.** 2002. Tauroursodeoxycholic acid, a bile acid, is neuroprotective in a transgenic animal model of Huntington's disease. Proc. Natl. Acad. Sci. U. S. A. **99:**10671-6.

45. **Kim, J. S., S. A. Reading, T. Brashers-Krug, V. D. Calhoun, C. A. Ross, and G. D. Pearlson.** 2004. Functional MRI study of a serial reaction time task in Huntington's disease. Psychiatry Res. **131:**23-30.

46. **Leavitt, B. R., C. L. Wellington, and M. R. Hayden.** 1999. Recent insights into the molecular pathogenesis of Huntington disease. Semin. Neurol. **19:**385-95.

47. **Lewin, A. S., K. A. Drenser, W. W. Hauswirth, S. Nishikawa, D. Yasumura, J. G. Flannery, and M. M. LaVail.** 1998. Ribozyme rescue of photoreceptor cells in a transgenic rat model of autosomal dominant retinitis pigmentosa. Nat. Med. **4:**967-71.

48. **Lewin, A. S., and W. W. Hauswirth.** 2001. Ribozyme gene therapy: applications for molecular medicine. Trends Mol. Med. **7:**221-8.

49. **Li, H., S. H. Li, Z. X. Yu, P. Shelbourne, and X. J. Li.** 2001. Huntingtin aggregate-associated axonal degeneration is an early pathological event in Huntington's disease mice. J. Neurosci. **21:**8473-81.

50. **Li, S. H., and X. J. Li.** 2004. Huntingtin and its role in neuronal degeneration. Neuroscientist **10:**467-75.

51. **Li, S. H., and X. J. Li.** 2004. Huntingtin-protein interactions and the pathogenesis of Huntington's disease. Trends Genet. **20:**146-54.

52. **Li, Y., T. Yokota, R. Matsumura, K. Taira, and H. Mizusawa.** 2004. Sequence-dependent and independent inhibition specific for mutant ataxin-3 by small interfering RNA. Ann. Neurol. **56:**124-9.

53. **MacDonald, M. E., S. Gines, J. F. Gusella, and V. C. Wheeler.** 2003. Huntington's disease. Neuromolecular Med. **4:**7-20.

54. **Mangiarini, L., K. Sathasivam, M. Seller, B. Cozens, A. Harper, C. Hetherington, M. Lawton, Y. Trottier, H. Lehrach, S. W. Davies, and G. P. Bates.** 1996. Exon 1 of the HD gene with an expanded CAG repeat is sufficient to cause a progressive neurological phenotype in transgenic mice. Cell **87:**493-506.

55. **McCampbell, A., J. P. Taylor, A. A. Taye, J. Robitschek, M. Li, J. Walcott, D. Merry, Y. Chai, H. Paulson, G. Sobue, and K. H. Fischbeck.** 2000. CREB-binding protein sequestration by expanded polyglutamine. Hum. Mol. Genet. **9:**2197-202.

56. **McCaw, E. A., H. Hu, G. T. Gomez, A. L. Hebb, M. E. Kelly, and E. M. Denovan-Wright.** 2004. Structure, expression and regulation of the cannabinoid receptor gene (CB1) in Huntington's disease transgenic mice. Eur. J. Biochem. **271:**4909-20.

57. **Miller, V. M., H. Xia, G. L. Marrs, C. M. Gouvion, G. Lee, B. L. Davidson, and H. L. Paulson.** 2003. Allele-specific silencing of dominant disease genes. Proc. Natl. Acad. Sci. U. S. A. **100:**7195-200.

58. **Naver, B., C. Stub, M. Moller, K. Fenger, A. K. Hansen, L. Hasholt, and S. A. Sorensen.** 2003. Molecular and behavioral analysis of the R6/1 Huntington's disease transgenic mouse. Neuroscience **122:**1049-57.

59. **Nellemann, C., K. Abell, A. Norremolle, T. Lokkegaard, B. Naver, C. Ropke, J. Rygaard, S. A. Sorensen, and L. Hasholt.** 2000. Inhibition of Huntington synthesis by antisense oligodeoxynucleotides. Mol. Cell. Neurosci. **16:**313-23.

60. **Norflus, F., A. Nanje, C. A. Gutekunst, G. Shi, J. Cohen, M. Bejarano, J. Fox, R. J. Ferrante, and S. M. Hersch.** 2004. Anti-inflammatory treatment with acetylsalicylate or rofecoxib is not neuroprotective in Huntington's disease transgenic mice. Neurobiol. Dis. **17:**319-25.

61. **O'Brien, T., and D. Lee.** 2004. Prospects for caspase inhibitors. Mini Rev. Med. Chem. **4:**153-65.

62. **Okun, M. S.** 2003. Huntington's disease: what we learned from the original essay. Neurologist **9:**175-9.

63. **Orr, H. T.** 2004. Neurodegenerative disease: neuron protection agency. Nature **431:**747-8.

64. **Pardridge, W. M.** 2001. Brain drug targeting and gene technologies. Jpn. J. Pharmacol. **87:**97-103.

65. **Parniewski, P., and P. Staczek.** 2002. Molecular mechanisms of TRS instability. Adv. Exp. Med. Biol. **516:**1-25.

66. **Perutz, M. F., T. Johnson, M. Suzuki, and J. T. Finch.** 1994. Glutamine repeats as polar zippers: their possible role in inherited neurodegenerative diseases. Proc. Natl. Acad. Sci. U. S. A. **91:**5355-8.

67. **Petersen, A., K. Mani, and P. Brundin.** 1999. Recent advances on the pathogenesis of Huntington's disease. Exp. Neurol. **157:**1-18.

68. **Qin, P. Z., and T. Dieckmann.** 2004. Application of NMR and EPR methods to the study of RNA. Curr. Opin. Struct. Biol. **14:**350-9.

69. **Rosenblatt, A., M. H. Abbott, L. M. Gourley, J. C. Troncoso, R. L. Margolis, J. Brandt, and C. A. Ross.** 2003. Predictors of neuropathological severity in 100 patients with Huntington's disease. Ann. Neurol. **54:**488-93.

70. **Ross, C. A., and M. A. Poirier.** 2004. Protein aggregation and neurodegenerative disease. Nat. Med. **10 Suppl:**S10-7.

71. **Sanchez Mejia, R. O., and R. M. Friedlander.** 2001. Caspases in Huntington's disease. Neuroscientist **7:**480-9.

72. **Sathasivam, K., C. Hobbs, L. Mangiarini, A. Mahal, M. Turmaine, P. Doherty, S. W. Davies, and G. P. Bates.** 1999. Transgenic models of Huntington's disease. Philos. Trans. R. Soc. Lond. B. Biol. Sci. **354:**963-9.

73. **Saudou, F., S. Finkbeiner, D. Devys, and M. E. Greenberg.** 1998. Huntingtin acts in the nucleus to induce apoptosis but death does not correlate with the formation of intranuclear inclusions. Cell **95:**55-66.

74. **Sawa, A.** 2001. Mechanisms for neuronal cell death and dysfunction in Huntington's disease: pathological cross-talk between the nucleus and the mitochondria? J. Mol. Med. **79:**375-81.

75. **Schaffar, G., P. Breuer, R. Boteva, C. Behrends, N. Tzvetkov, N. Strippel, H. Sakahira, K. Siegers, M. Hayer-Hartl, and F. U. Hartl.** 2004. Cellular toxicity of polyglutamine expansion proteins: mechanism of transcription factor deactivation. Mol. Cell. **15:**95-105.

76. **Schubert, S., and J. Kurreck.** 2004. Ribozyme- and deoxyribozyme-strategies for medical applications. Curr. Drug Targets **5:**667-81.

77. **Shimayama, T., S. Nishikawa, and K. Taira.** 1995. Generality of the NUX rule: kinetic analysis of the results of systematic mutations in the trinucleotide at the cleavage site of hammerhead ribozymes. Biochemistry **34:**3649-54.

78. **Sieradzan, K. A., and D. M. Mann.** 2001. The selective vulnerability of nerve cells in Huntington's disease. Neuropathol. Appl. Neurobiol. **27:**1-21.

79. **Sugars, K. L., and D. C. Rubinsztein.** 2003. Transcriptional abnormalities in Huntington disease. Trends Genet. **19:**233-8.

80. **Tenenbaum, L., A. Chtarto, E. Lehtonen, T. Velu, J. Brotchi, and M. Levivier.** 2004. Recombinant AAV-mediated gene delivery to the central nervous system. J. Gene Med. **6 Suppl 1:**S212-22.

81. **The Huntington's Disease Collaborative Research Group**.1993. A novel gene containing a trinucleotide repeat that is expanded and unstable on Huntington's disease chromosomes. Cell **72:**971-83.

82. **Tuschl, T.** 2001. RNA interference and small interfering RNAs. Chembiochem. **2:**239-45.

83. **Tuschl, T., and A. Borkhardt.** 2002. Small interfering RNAs: a revolutionary tool for the analysis of gene function and gene therapy. Mol. Interv. **2:**158-67.

84. **von Horsten, S., I. Schmitt, H. P. Nguyen, C. Holzmann, T. Schmidt, T. Walther, M. Bader, R. Pabst, P. Kobbe, J. Krotova, D. Stiller, A. Kask, A. Vaarmann, S. Rathke-Hartlieb, J. B. Schulz, U. Grasshoff, I. Bauer, A. M. Vieira-Saecker, M. Paul, L. Jones, K. S. Lindenberg, B. Landwehrmeyer, A. Bauer, X. J. Li, and O. Riess.** 2003. Transgenic rat model of Huntington's disease. Hum. Mol. Genet. **12:**617-24.

85. **Walling, H. W., J. J. Baldassare, and T. C. Westfall.** 1998. Molecular aspects of Huntington's disease. J. Neurosci. Res. **54:**301-8.

86. **Wang, C. H., D. W. Liu, Y. P. Tsao, X. Xiao, and S. L. Chen.** 2004. Can genes transduced by adeno-associated virus vectors elicit or evade an immune response? Arch. Virol. **149:**1-15.

87. **Wanker, E. E.** 2000. Protein aggregation in Huntington's and Parkinson's disease: implications for therapy. Mol. Med. Today **6:**387-91.

88. **Wellington, C. L., and M. R. Hayden.** 2000. Caspases and neurodegeneration: on the cutting edge of new therapeutic approaches. Clin. Genet. **57:**1-10.

89. **Wellington, C. L., B. R. Leavitt, and M. R. Hayden.** 2000. Huntington disease: new insights on the role of huntingtin cleavage. J. Neural. Transm. Suppl.**:**1-17.

90. **Wexler, N. S., J. Lorimer, J. Porter, F. Gomez, C. Moskowitz, E. Shackell, K. Marder, G. Penchaszadeh, S. A. Roberts, J. Gayan, D. Brocklebank, S. S. Cherny, L. R. Cardon, J. Gray, S. R. Dlouhy, S. Wiktorski, M. E. Hodes, P. M. Conneally, J. B. Penney, J. Gusella, J. H. Cha, M. Irizarry, D. Rosas, S. Hersch, Z. Hollingsworth, M. MacDonald, A. B. Young, J. M. Andresen, D. E. Housman, M. M. De Young, E. Bonilla, T. Stillings, A. Negrette, S. R. Snodgrass, M. D. Martinez-Jaurrieta, M. A. Ramos-Arroyo, J. Bickham, J. S. Ramos, F. Marshall, I. Shoulson, G. J. Rey, A. Feigin, N. Arnheim, A. Acevedo-Cruz, L. Acosta, J. Alvir, K. Fischbeck, L. M. Thompson, A. Young, L. Dure, C. J. O'Brien, J. Paulsen, A. Brickman, D. Krch, S. Peery, P. Hogarth, D. S. Higgins, Jr., and B. Landwehrmeyer.** 2004. Venezuelan kindreds reveal that genetic and environmental factors modulate Huntington's disease age of onset. Proc. Natl. Acad. Sci. U. S. A. **101:**3498-503.

91. **Xia, H., Q. Mao, S. L. Eliason, S. Q. Harper, I. H. Martins, H. T. Orr, H. L. Paulson, L. Yang, R. M. Kotin, and B. L. Davidson.** 2004. RNAi suppresses polyglutamine-induced neurodegeneration in a model of spinocerebellar ataxia. Nat. Med. **10:**816-20.

92. **Yamamoto, A., J. J. Lucas, and R. Hen.** 2000. Reversal of neuropathology and motor dysfunction in a conditional model of Huntington's disease. Cell **101:**57-66.

93. **Yen, L., S. M. Strittmatter, and R. G. Kalb.** 1999. Sequence-specific cleavage of Huntingtin mRNA by catalytic DNA. Ann. Neurol. **46:**366-73.

94. **Zdzienicka, E., M. Rakowicz, H. Mierzewska, D. Hoffman-Zacharska, T. Jakubowska, R. Poniatowska, A. Sulek, E. Waliniowska, U. Zalewska, J. Kulczycki, and J. Zaremba.** 2002. [Clinical and genetic study of juvenile form of Huntington's disease]. Neurol. Neurochir. Pol. **36:**245-58.

95. **Zhang, Y., M. Li, M. Drozda, M. Chen, S. Ren, R. O. Mejia Sanchez, B. R. Leavitt, E. Cattaneo, R. J. Ferrante, M. R. Hayden, and R. M. Friedlander.** 2003. Depletion of wild-type huntingtin in mouse models of neurologic diseases. J. Neurochem. **87:**101-6.

96. **Zhang, Y. C., M. M. Taylor, W. K. Samson, and M. I. Phillips.** 2005. Antisense inhibition: oligonucleotides, ribozymes, and siRNAs. Methods Mol. Med. **106:**11-34.

97. **Zielonka, D., M. de Mezer, A. Niezgoda, K. Reperowicz, W. Krzyzosiak, and W. Kozubski.** 2002. [Clinical picture of patients with Huntington's disease in relation to the number of trinucleotide CAG repeats in IT-15 gene]. Neurol. Neurochir. Pol. **36:**903-9.

98. **Zuccato, C., M. Tartari, A. Crotti, D. Goffredo, M. Valenza, L. Conti, T. Cataudella, B. R. Leavitt, M. R. Hayden, T. Timmusk, D. Rigamonti, and E. Cattaneo.** 2003. Huntingtin interacts with REST/NRSF to modulate the transcription of NRSE-controlled neuronal genes. Nat. Genet. **35:**76-83.

BIOGRAPHICAL SKETCH

I was born in the small municipality of Arroyo, Puerto Rico in January 27th of 1976. I graduated with honors from the University High School, Puerto Rico, after which I attended the University of Central Florida for four years. After receiving my Bachelor of Science degree from the University of Central Florida I worked for one year in the laboratory of Dr. Cristina Fernandez-Valle. In 1999 I began graduate studies in the Interdisciplinary Program for Biomedical Sciences at the University of Florida while also becoming the proud father of Arianna Lee Rodriguez. Under the guidance and mentoring of Dr. Ronald J. Mandel I began to pursue my doctoral degree during the spring of 2000 at which time I was also awarded a five-year pre-doctoral fellowship from National Institute of Neurological Disorders and Stroke.